UNIVERSITY *of York*

This is a repository copy of *Mesomorphism and Photophysics of Some Metallomesogens Based on Hexasubstituted 2,2':6', 2''-Terpyridines:6', 2''-Terpyridines*.

White Rose Research Online URL for this paper:
https://eprints.whiterose.ac.uk/100378/

Version: Accepted Version

Article:

White Rose
university consortium
Universities of Leeds, Sheffield & York

eprints@whiterose.ac.uk
https://eprints.whiterose.ac.uk/

Mesomorphism and Photophysics of some Metallomesogens based on Hexasubstituted 2, 2': 6', 2''-Terpyridines

N. S. Saleesh Kumar[†], Marsel Z. Shafikov[§], Adrian C. Whitwood[†],

Bertrand Donnio[‡], Peter B. Karadakov[†],

Valery N. Kozhevnikov[†,#] and Duncan W. Bruce[†,*]

[†] *Department of Chemistry, University of York, Heslington, YORK YO10 5DD (UK)*
Tel: (+44) 1904 324085; E-mail: duncan.bruce@york.ac.uk

[§] *Laboratory of Organic Materials, Institute of Organic Synthesis, Ural Federal University, Mira 19, Ekaterinburg, 620002, Russia.*

[‡] *Institut de Physique et Chimie des Matériaux de Strasbourg (IPCMS), CNRS-Université de Strasbourg (UMR 7504), 23 rue du Loess BP 43, 67034 STRASBOURG Cedex 2, FRANCE*

[#] *Present address: School of Life Sciences, Northumbria University, Newcastle-Upon-Tyne, NE1 8ST, UK.*

Abstract:

The luminescent and mesomorphic properties of a series of metal complexes based on hexacatenar 2,2′:6′,2′′terpyridines are investigated using experimental methods and density functional theory (DFT). Two types of ligand are examined, namely 5,5′′-di(3,4,5-trialkoxyphenyl)terpyridine with or without a fused cyclopentene ring on each pyridine and their complexes were prepared with the following transition metals: Zn^{II}, Co^{III}, Rh^{III}, Ir^{III}, Eu^{III}and Dy^{III}. The exact geometry of some of these complexes was determined by single X-ray diffraction analysis. All complexes with long alkyl chains were found to be liquid crystalline, which property was induced on complexation. The liquid-crystalline behaviour of the complexes was studied by polarizing optical microscopy and small-angle X-ray diffraction. Some of the transition metal complexes (for example, those with Zn^{II} and Ir^{III}) are luminescent in solution, the solid state and the mesophase; their photophysical properties were studied both experimentally and using DFT methods (M06-2X and B3LYP).

Graphic Abstract:
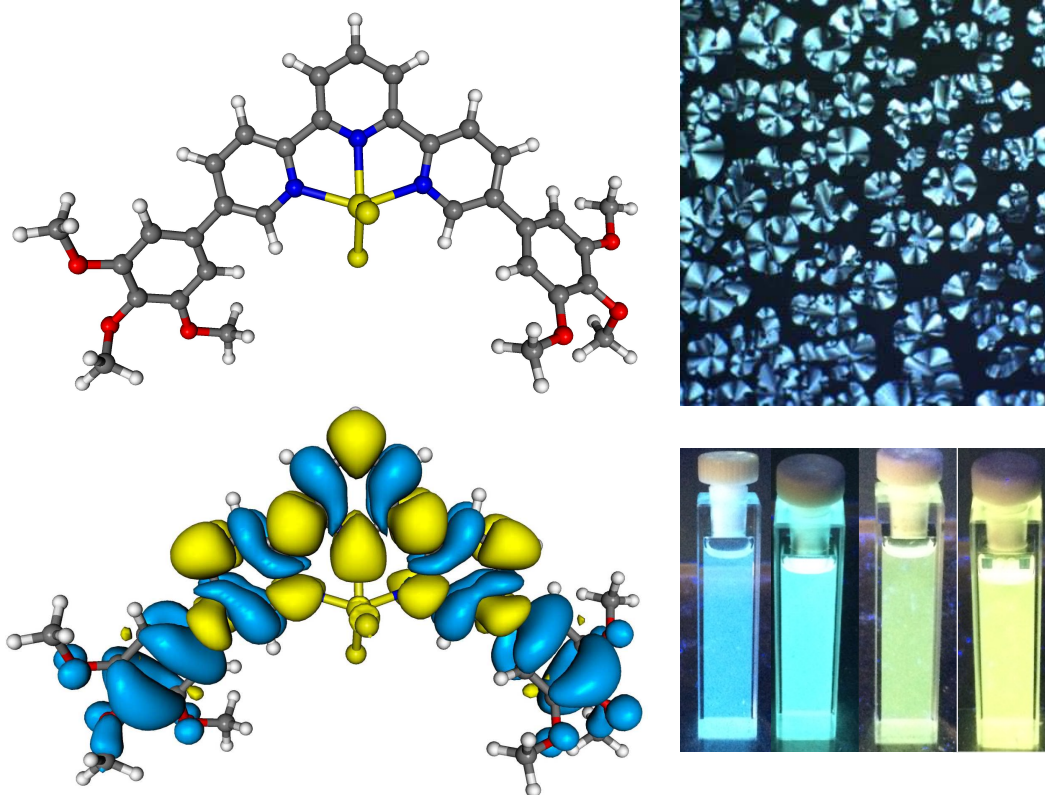
Introduction

Molecular coordination compounds are very versatile materials owing, *inter alia*, to their diverse coordination geometries, variable oxidation states and photochemical and photophysical responses. Major areas of application include catalysis,[1] molecular wires and switches,[2] photovoltaic cells,[3] organic light-emitting devices,[4] and active electron-transporting agents in natural and artificial systems.[5] The role of metal complexes in display devices is a topic of a on-going interest and, while much commercial interest is centred around emissive Ir[III] complexes,[6] there is a broader interest in emissive materials incorporating, for example, Pt[II(7)] and Cu[I].[8]

The introduction of luminescent (*d*- and *f*-block metal complexes) liquid crystals[7e-g,9] has been an interesting challenge in this area. Liquid crystals represent materials with inherent order that could lead to preferred conduction pathways (lower display drive voltages) or polarised emission, and their fluid nature gives the potential for self healing. However, while square-planar Pt[II] complexes are rather readily modified to give liquid crystal phases, elements requiring higher coordination numbers (Ir[III], lanthanides) represent a different level of challenge.[6a-b,10]

N-Heterocyclic ligands have proved very versatile in the synthesis of functional metal complexes, and the availability of a range of such ligands depends on good synthetic accessibility. Of particular note is inverse electron demand Diels-Alder chemistry (so-called Boger reaction), which represents a very flexible way into a range of substituted pyridines such as 2-phenylpyridines, 1,3-di(2-pyridyl)benzenes and terpyridines.[11] Of these, terpyridines[12] are very attractive ligands for a range of transition metals and, as we now show, suitably functionalised derivatives show great versatility in endowing liquid crystal properties upon a range of metal complexes with five-, six- and nine-coordinate geometries. More than that, many resultant complexes are emissive, with singlet or triplet emission some of which is very efficient.

Thus, the synthesis is reported of a series of 5,5′′-disubstituted terpyridine metallomesogens formed by complexing the terpy ligands **8**-*n* and **9**-*n* with simple salts of zinc(II), the d^6 metals iridium(III) and rhodium(III), dysprosium(III) and europium(III) as examples of lanthanide complexes, and a novel (from a metallomesogen point of view) 2 : 1 complex of cobalt(III). Some of the complexes are luminescent both in solution and the solid state and a detailed analysis of their liquid-crystalline and photophysical properties are now described, supported by a computational study of the photophysical properties of the zinc(II) complexes.
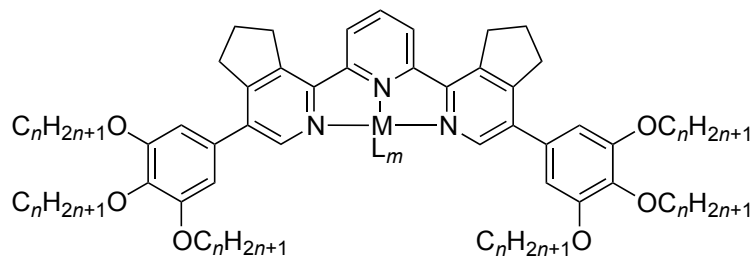
Synthesis

Thus, Boger chemistry forms the basis for the present study and Scheme 1 shows the synthetic strategy adopted for the synthesis of terpyridines employed. It starts with the condensation of a hydrazone oxime precursor (**1**-1) with pyridine-2,6-dicarboxaldehyde to give triazine **3**-1, which is then reacted with 2,5-norbornadiene or 1-morpholinocyclopentene to give pyridines **4**-1 and **5**-1, respectively. Long alkyl chains were then introduced by the cleavage of methyl ether bond using BBr_3 in dichloromethane followed by *O*-alkylation using 1-bromoalkanes under standard conditions. The final complexes (Figure 1) were then obtained by reaction with the appropriate metal salts following literature methods. The detailed procedures for the preparation of the ligands and final complexes are provided in the Supporting Information.

Single Crystal Characterisation

In order to probe the coordination geometries of these materials, single crystals were obtained for methoxy derivatives as the short chains increase the tendency for formation of good-quality crystals. Complexes of Dy^{III}, Eu^{III} and Co^{III} were therefore characterised crystallographically, while two different structures were obtained for complexes of Zn^{II}. Crystallographic parameters are collected in Table 1.
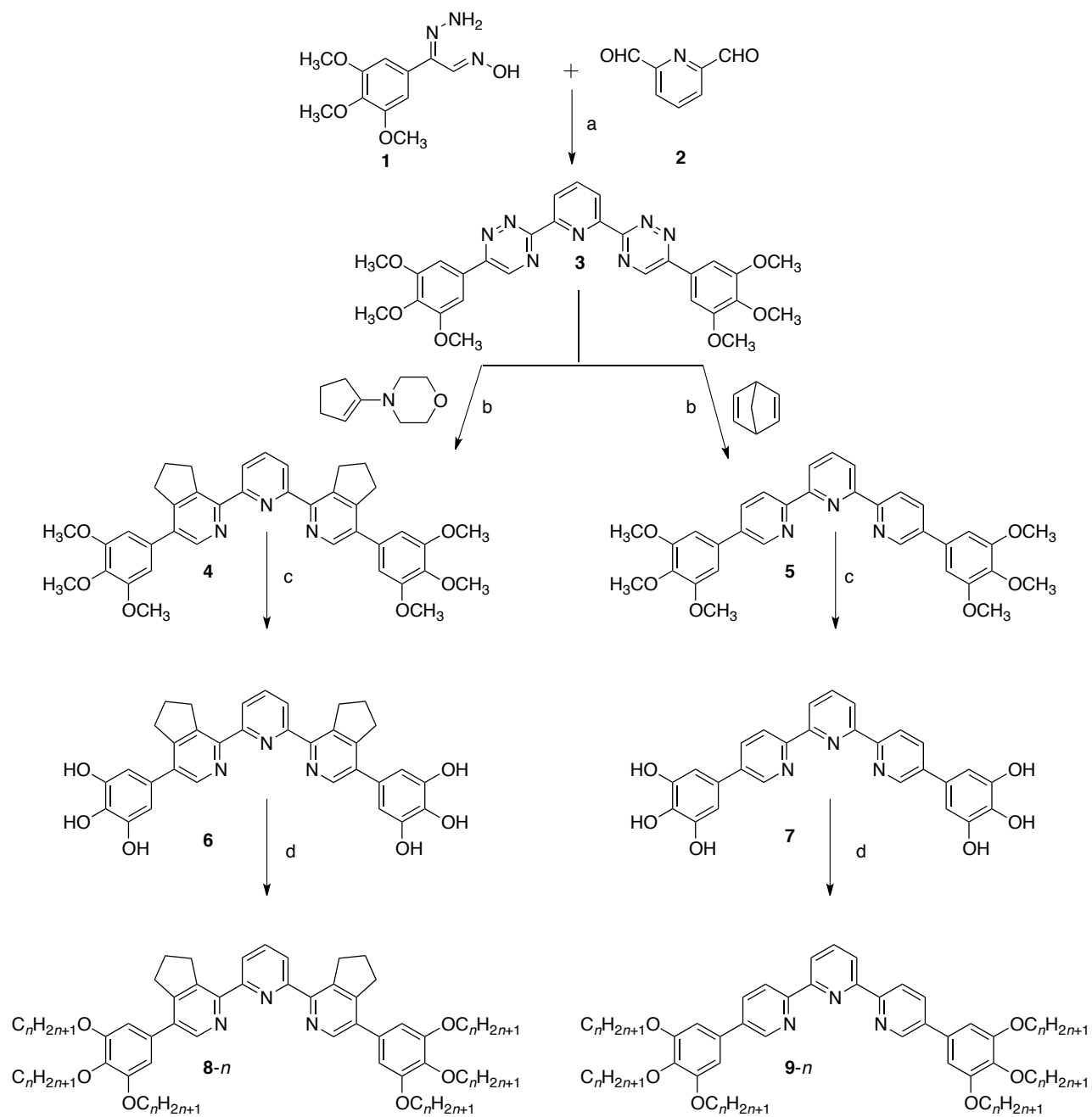
Scheme 1. Synthesis of terpyridines: *Reagents and Conditions*: a) acetic acid, 118 °C; b) xylene, reflux under pressure; c) BBr$_3$, CH$_2$Cl$_2$, room temperature; d) C$_n$H$_{2n+1}$Br, K$_2$CO$_3$, DMF, 100 °C.

10-*n*: ZnCl$_2$
12-*n*: RhCl$_3$
13-*n*: IrCl$_3$

16-*n*: Eu(κ^2-NO$_3$)$_3$(OH$_2$)
17-1: Dy(κ^2-NO$_3$)$_3$(OH$_2$)
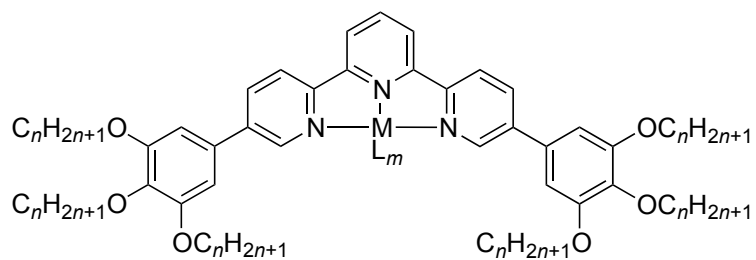
11-*n*: ZnCl$_2$
14-*n*: RhCl$_3$

15-*n*: IrCl$_3$
18-16: Eu(κ^2-NO$_3$)$_3$(OH$_2$)
19-12: Dy(κ^2-NO$_3$)$_3$(OH$_2$)
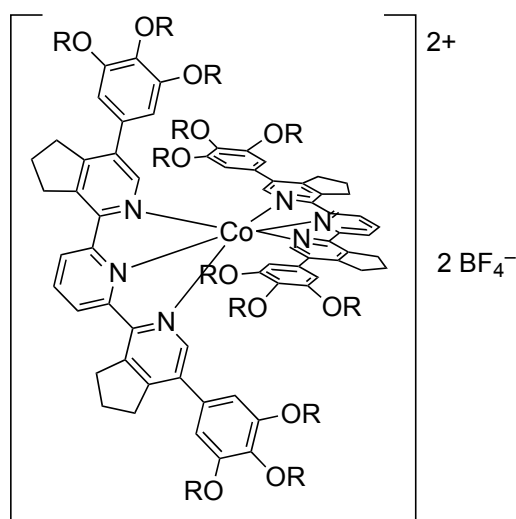
20: M = Co; R = C$_{16}$H$_{33}$
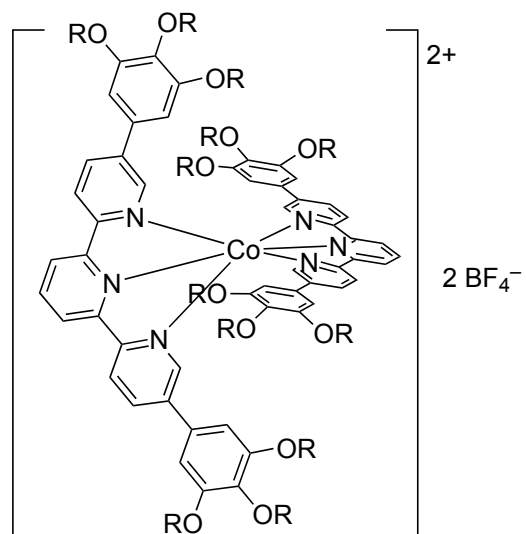
21: M = Co; R = C$_{16}$H$_{33}$

Figure 1. The structure of metal complexes synthesised in this work.

Table 1   Single crystal X-ray diffraction data for complexes **10**-1 (2 structures), **16**-1, **17**-1 and **20**-1.

	10-1 (first structure)	**10**-1 (second structure)	**16**-1	**17**-1	**20**-1
CCDC Reference Number	1415907	1415908	1415909	1415910	1415911
Empirical formula	$C_{39}H_{39}Cl_2N_3O_6Zn$	$C_{39}H_{39}Cl_2N_3O_6Zn$	$C_{47}H_{61.55}EuN_6O_{19.23}$	$C_{45}H_{54}DyN_7O_{17}$	$C_{82}H_{94}B_2CoF_8N_6O_{16}$
Formula weight/g mol^{-1}	782.00	782.00	1170.23	1127.45	1652.18
T/K	110(2)	110(2)	110(2)	110(2)	110(2)
Crystal system	Triclinic	Monoclinic	Monoclinic	Triclinic	Monoclinic
Space group	P-1	P2(1)/c	P2(1)	P-1	C2/c
Unit cell dimensions/Å	a = 8.8783(9)	a = 20.5916(16)	a = 9.8154(8)	a = 11.4294(7)	a = 34.4177(15)
	b = 15.3595(15)	b = 24.430(2)	b = 21.7325(17)	b = 14.7897(9)	b = 11.6210(2)
	c = 16.5288(16)	c = 17.0046(13)	c = 12.2713(10)	c = 15.0025(9)	c = 26.5242(12)
α/°	68.658(2)	90	90	107.7170(10)	90
β/°	87.706(2)	103.745(2)	94.080(2)	93.0590(10)	129.018(7)
γ/°	81.434(2)	90	90	96.9850(10)	90
Volume/ $Å^3$	2075.74	8309.4(11)	2611.0(4)	2386.8(3)	8242.5(8)
Z	2	8	2	2	4
ρ_{calc}/Mg m^{-3}	1.251	1.250	1.483	1.569	1.331
Absorption coefficient/mm^{-1}	0.765	0.765	1.281	1.646	2.368
$F(000)$	812	3248	1197.0	1150	3460
Crystal size/mm^3	0.32 x 0.20 x 0.05	0.37 x 0.31 x 0.04	0.14 x 0.06 x 0.05	0.26 x 0.06 x 0.02	0.2049 x 0.1371 x 0.082
θ range for data collection	1.32 to 28.31°	1.02 to 25.03°	1.66 to 28.29°	1.46 to 28.31°	8.296 to 143.024°
Index ranges	$-11 \leq h \leq 11$, $-20 \leq k \leq 19$,	$-24 \leq h \leq 23$, $0 \leq k \leq 29$,	$-13 \leq h \leq 13$, $-28 \leq k \leq 28$,	$-15 \leq h \leq 15$, $-19 \leq k \leq 19$,	$-41 \leq h \leq 40$, $-14 \leq k \leq 6$,
	$-22 \leq l \leq 22$	$0 \leq l \leq 20$	$-15 \leq l \leq 16$	$-19 \leq l \leq 20$	$-32 \leq l \leq 30$
Reflections collected	20500	14664	26692	21193	16046
Independent reflections	10131 [$R_{(int)}$ = 0.0255]	14664 [$R_{(int)}$ = 0.0000]	12748 [$R_{(int)}$ = 0.0319]	11592 [$R_{(int)}$ = 0.0252]	7852 [$R_{(int)}$ = 0.0282]
Completeness (%) to (θ)	98.3 to 56.62	99.8 to 50.06	99.8 to 56.58	97.5 to 56.62	99.92 to 66.97
Max. and min. transmission	0.960 and 0.724	0.970 and 0.599	0.938 and 0.794	0.9678 and 0.6742	-
Data/restraints/parameters	10131 / 0 / 466	14664 / 0 / 931	12748 / 5 / 695	11592 / 0 / 646	7852 / 38 / 593
Goodness-of-fit on F^2	1.031	1.020	0.979	1.028	1.046
Final R indices [$I > 2\sigma(I)$]	R_1 = 0.0374, wR_2 = 0.0965	R_1 = 0.0427, wR_2 = 0.1130	R_1 = 0.0321, wR_2 = 0.0604	R_1 = 0.0322, wR_2 = 0.0716	R_1 = 0.0505, wR_2 = 0.1316
R indices (all data)	R_1 = 0.0503, wR_2 = 0.1005	R_1 = 0.0576, wR_2 = 0.1201	R_1 = 0.0399, wR_2 = 0.0628	R_1 = 0.0418, wR_2 = 0.0757	R_1 = 0.0676, wR_2 = 0.1423
Largest diff. peak and hole	0.659 and -0.454	0.799 and -0.593	1.075 and -0.459	1.398 and -0.546	1.24 and -0.38

***Zinc Complex 10**-1 (structure 1)*

This complex shows the expected distorted trigonal bipyramidal geometry around zinc with the two chloride ligands and the central ring nitrogen forming the trigonal plane (Figure 2). The length of the bond between the zinc and this central nitrogen is 2.1191(14) Å, which is shorter than those to the other nitrogens, which are equivalent statistically at 2.1377(15) and 2.1481(15) Å. There is also a small degree of dissymmetry in the two Zn–Cl distances at 2.2854(6) and 2.2534(5) Å although, as the difference is about 1.5%, this is a small effect. The Cl–Zn–Cl angle is 117.07(2)°. The parameters for the two chloride ligands around zinc are very similar to those reported previously for structurally related complexes based on bis(iminomethyl)pyridyl complexes (Figure 3). These complexes also show a shorter Zn–N bond to the central nitrogen, but given the chemically different nature of the bound nitrogens in the iminomethylpyridine complex, the difference in bond lengths is greater.[13]
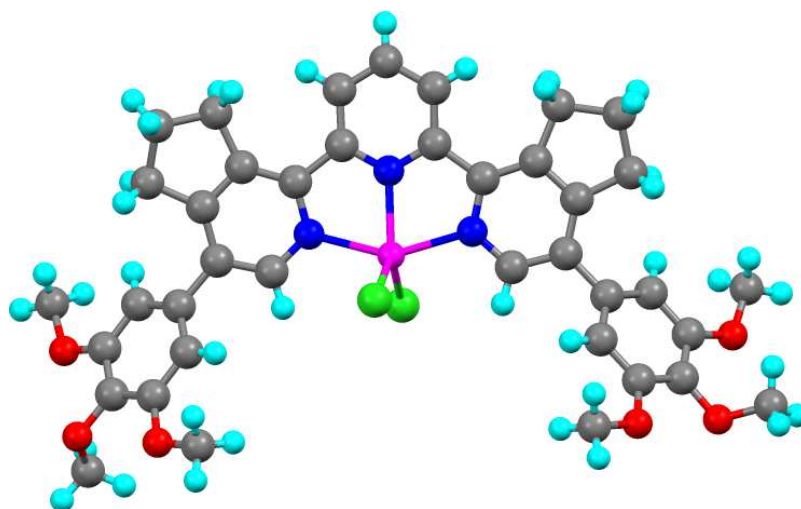
Figure 2. Single crystal X-ray structure of complex **10**-1.

Despite the steric pressure of the α-methylene hydrogens in the fused cyclopentene ring, the three pyridyl rings are very close to co-planar with angles of 6 and 7° between the plane defined by the central pyridine ring and those of the two outer pyridine rings.
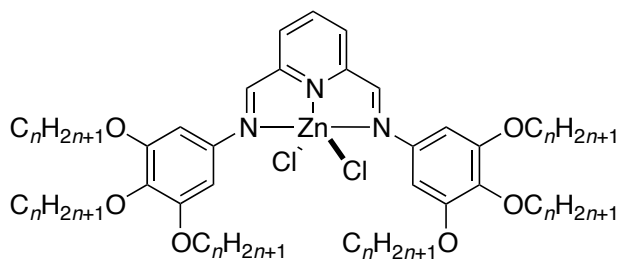
Figure 3   The related bis(iminomethyl)pyridine complex of dichlorozinc(II).

The complexes pack in a back-to-back fashion along the a-axis (Figure 4) and the distance between the planes of two central pyridine rings in neighbouring complexes is 3.315(3) Å, although there are no obvious intermolecular π-π interactions (by observing down the a-axis). Such a back-to-back motif, which represents efficient space filling to accommodate the alkoxy chains, was also characteristic of the bis(iminomethyl)pyridine complexes mentioned earlier.[13]
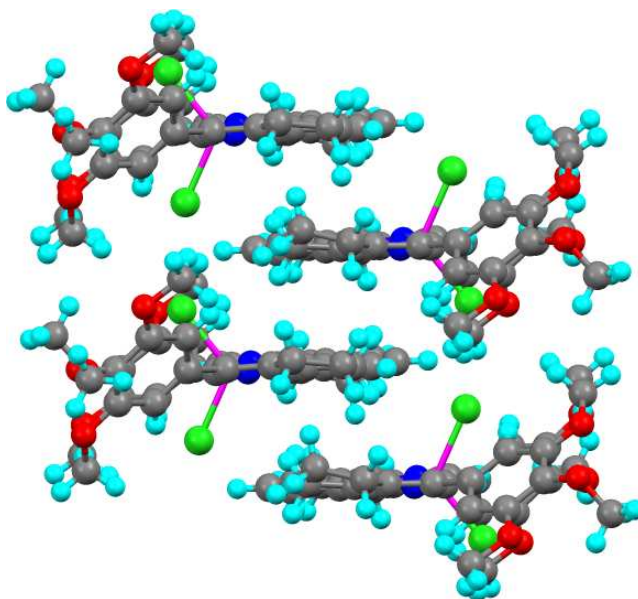
Figure 4   Side view showing the back-to-back packing of complex **10**-1 along the crystallographic a-axis

Zinc Complex 10-1 (structure 2)

Whereas the structure for **10**-1 above (space group $P\bar{1}$) was obtained from a crystal grown from CHCl₃, this crystal ($P21/c$) came out of a MeOH/EtOAc mixture with two complexes in the asymmetric unit. This new crystal contained disordered solvent in a channel for which a suitable

model could not be determined and its effect was therefore removed using the SQUEEZE algorithm.[14] The two molecular units (Fig. S1) are rather similar except that in one, the two Zn–Cl distances are now equal (2.2741(9) and 2.2725(8) Å with the angle at zinc = 114.62(3)°), whereas in the other they are different (2.2867(8) and 2.2603(8) Å with the angle at zinc = 112.03(3)°). Both show unsymmetric Zn–N distances, which is now more pronounced in complex 1 (2.122(2), 2.146(3) and 2.168(2) Å) compared to complex 2 (2.166(2), 2.146(2) and 2.145(2) Å)). The back-to-back stacking is still present (Fig. S1c) except that the mutual disposition of neighbouring complexes is slightly different and the complexes are stacked in groups of four so that the arrangement is Zn2···Zn1···Zn1···Zn2. Thus the pyridyl rings between the two Zn1 complexes are parallel and separated by 3.309(4) Å, but the pyridyl rings in the two Zn2 are not parallel, rather the two planes make an angle of around 6° with a centroid-to-centroid difference of 3.5167(15) Å.

Europium Complex 16-1

This complex was obtained from 2-ethoxyethanol/diethyl ether as a ten-coordinate complex with europium bound by the tridentate terpyridine, three κ^2-nitrates and a water molecule. The asymmetric unit included two areas of disordered solvent containing water, ether and ethoxyethanol, with many of the ether and ethoxyethanol molecules occupying similar sites. One of the areas included either ether and water (26%) or an ethoxyethanol (74%). The second was either an ether (78%) or an ethoxyethanol (22%) The relative occupancies were refined. Some water O-H bond lengths were constrained to 0.958 Å (O16 -H16a, O21-H21a, O21-H21b), while the O-H bond length for one ethoxyethanol was constrained to 0.82 Å (O18-H18a). The C47a-O20 bond length was restrained to be 1.41 Å. The molecular structure, shown in Figure 5 and without solvent of crystallisation for clarity, is rather similar to that of the dysprosium complex below although it is clear that the solvent of crystallisation plays a space-filling role if the structure is built up.

There is significant dissymmetry in the coordination of the terpyridine ligand and this time it is one of the outer nitrogens that shows the shortest bond length to Eu at 2.568(4) Å while the

central pyridine nitrogen-Eu distance is the longest at 2.622(4) Å, the remaining outer Eu–N bond length being 2.601(2) Å. The binding of the nitrate anions is also unsymmetric with pairs of Eu–O distances at: 2.581(4) and 2.599(3) Å, 2.535(4) and 2.470(3) Å, and 2.494(3) and 2.466(4) Å. The Eu–O distance in the coordinated water is 2.387(3) Å. However, the twist angles between the plane of the central pyridine ring and the two outer pyridine rings are rather similar at 24.76(17)° and 23.21(18)°, in contrast to the situation with the Zn and Dy complexes.
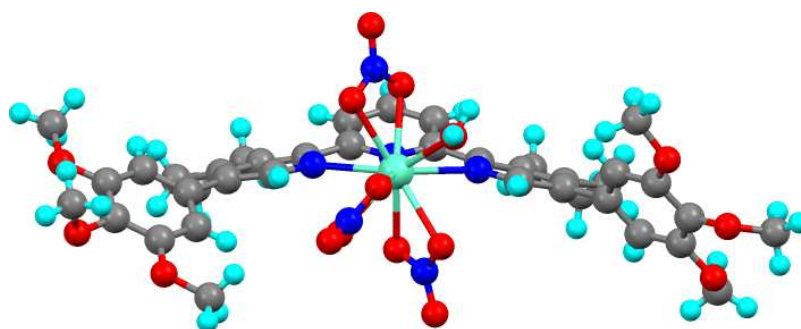
Figure 5   Molecular structure of the Eu complex **16**-1.

Dysprosium Complex 17-1

Crystals of this ten-coordinate complex were obtained from a two-solvent system of acetonitrile and ether, and a molecule of each was found within the crystal lattice (Figure 6a and 6b). The ten-fold coordination was made up of the tridentate terpyridine, three bidentate nitrate ions and a water molecule. As with the zinc complexes above, the bond between the metal and the central pyridine nitrogen is observed to be shorter (2.516(2) Å) than the other two metal-nitrogen bonds (lengths of 2.549(2) and 2.541(2) Å). Similarly to zinc complexes, each nitrate shows some degree of dissymmetry in the Dy–O bond lengths: 2.448(2) and 2.490(2) Å, 2.563(2) and 2.525(2), and 2.476(3) and 2.447(2) Å. Another interesting feature is the twisting of the pyridyl rings so that in common with the zinc complex above, the central pyridyl ring is twisted out of co-planarity by *ca* 9° (*cf* 6° and 7° for Zn) with respect to one of the outer pyridyls but by almost 32° with respect to the other. As coordination around Zn^{II} and Dy^{III} is not metal orbital-directed, then the origin of the effect is not immediately clear until the complex is viewed as a space-filling image whereupon a relatively short N···H interaction (2.58 Å) between an acetonitrile solvent molecule and the γ-

hydrogen of the central pyridine ring becomes obvious, which prevents the adjacent ring from achieving a co-planar orientation (Figure 6c).
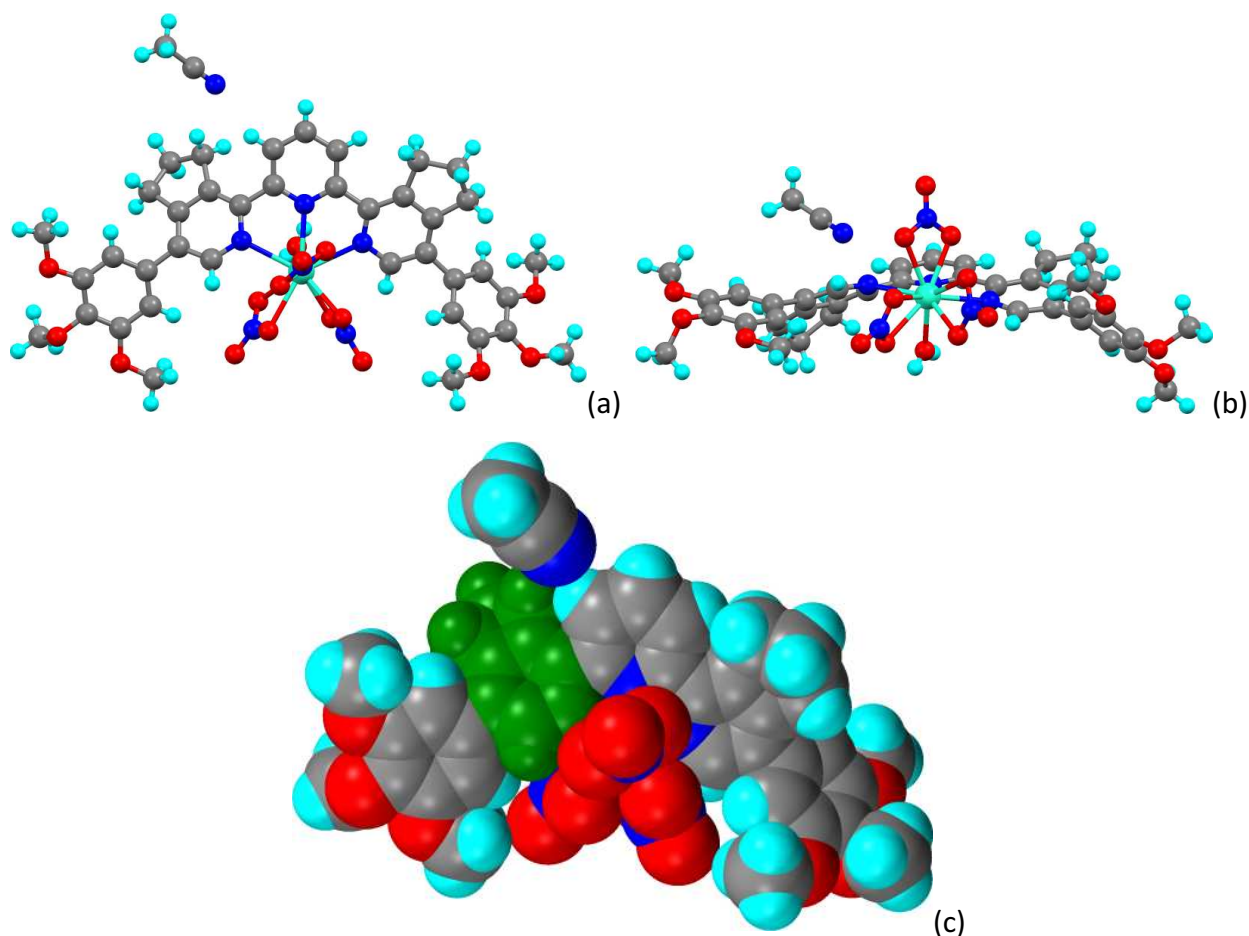
Figure 6   Views of the Dy complex **17**-1: (a) from the top, (b) from the side and (c) as a space-filling model to highlight the acetonitrile⋯pyridyl hydrogen interaction with the ring twisted out of plane shown in green. The solvating ether molecule does not interact with the complex and is omitted for clarity.

Cobalt Complex 20-1

The crystal obtained was disordered with the complex, anion and solvent affected. The complex exhibited disorder of the pyridyl and fused cyclopentene rings as well as one of the methoxy groups. The *m*- and *p*-carbons of the pyridyl were modelled in two position of equal occupancy and the corresponding atomic displacement parameters (ADPs) were, *e.g.* C11a and C11b. For the cyclopentene rings, the carbon opposite the double bond was modelled in two positions again with equal occupancies and constrained ADPs, *e.g.* C5a and C5b. For one of the methoxy groups,

the carbon was modelled in two positions with equal occupancies and constrained ADPs C38A and C38b.

The BF_4^- anion was modelled in two positions with refined occupancies of 0.756:0.244(7). The ADPs of three pairs of atoms were constrained to be equal, namely F1A and F1B, F4A and F4B, and B1A and B1B. The B–F bond lengths were constrained to be 1.40 Å. The F···F distances within each BF_4^- anion were constrained to be equal. One methanol of crystallisation was disordered and modelled in two positions with equal occupancies. There was also a zone of disordered electron density, which presumably contains a mixture of disordered solvent and a disordered BF_4^- anion for which a discrete model could not be obtained so it was accounted for using a solvent mask. The volume was 161.5 $Å^3$ with an estimated electron count of 49.7. This is consistent with a composition of one BF_4^- anion and one methanol.

The complex then shows the two terpyridines coordinated to the Co[III] centre and the mode of coordination is illustrated in Figure 7a (the solvent and anions have been removed for clarity). The two terpyridines are symmetry related so that there is, for example, one set of Co–N distances, the shortest of which is the distance between Co and the N of the central pyridine (1.8557(19) Å) whereas the other two are slightly longer (1.9326(19) and 1.9436(19) Å). The N-Co-N angles are 179.94(13)° for the two central pyridine nitrogens and 165.16(7)° for the other two.

The complexes are organised by stacking one upon another in the *b*-direction with the space in between being occupied by the subsequent stack in the *c*-direction (Figure 7b).

(a)

(b)
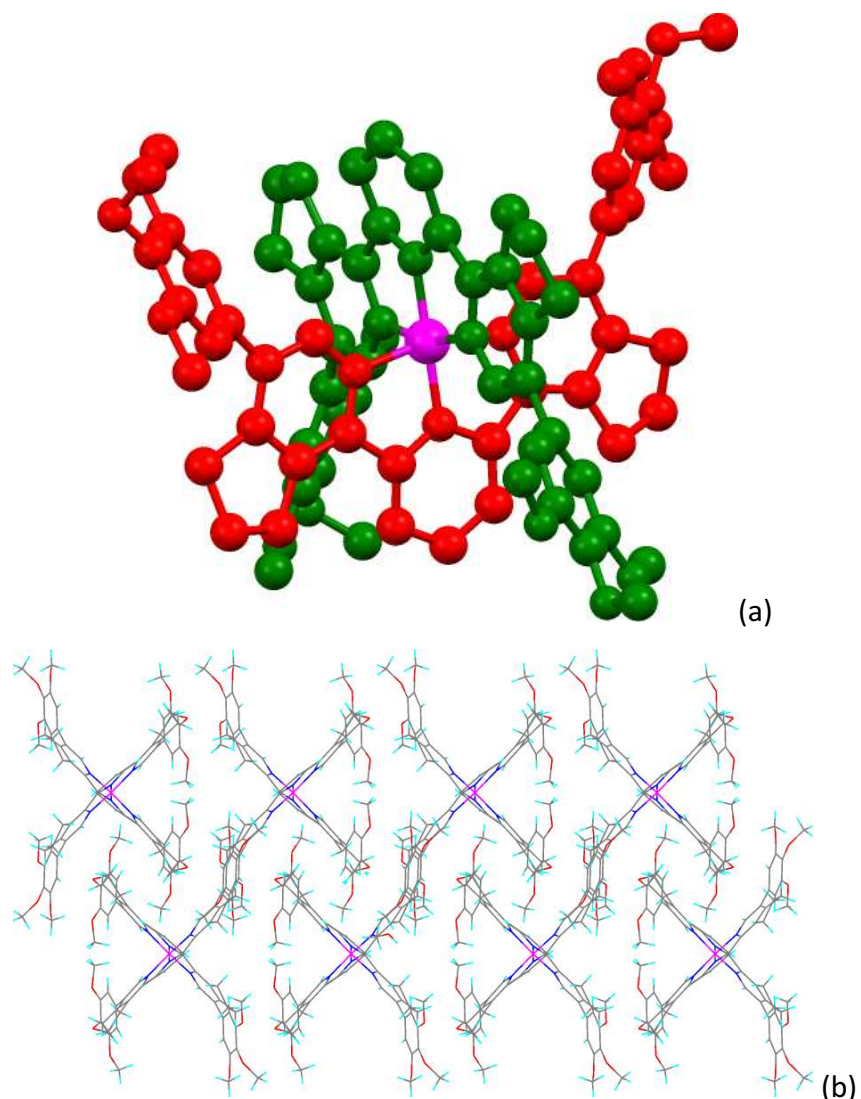
Figure 7 (a) Molecular structure of complex **20**-1 with hydrogens and alkyl chains omitted showing the disposition of the two terpyridine ligands around the cobalt centre; (b) view of the packing of **20**-1 in the solid state viewed down the *a*-axis.

It should be noted that there is a recent report[17b] of single crystal X-ray structures of 2:1 terpy-cobalt(II) complexes, noted as 'metallomesogenic precursors', in which various intermolecular interactions were analysed in some detail.

Mesomorphic Properties

The mesomorphic properties of the metal complexes were investigated by polarised optical microscopy (POM), small-angle X-ray scattering (SAXS) and DSC for which it was often difficult to

get useful data (something we have occasionally found over many years working with metallomesogens and for which we have no useful explanation); some indicative traces are found in the SI. It is important to mention that the ligands are not liquid-crystalline in nature and therefore that the mesophases are induced and stabilised by metal complexation.[15] All the complexes described here showed enantiotropic columnar phases and the detailed phase transitions are summarised in Table 2, while X-ray data are collected in Table 3; diffraction patterns not shown in Figure 10 are found in Figure S6.

Zn^{II} complexes

All higher homologues of Zn^{II} complexes prepared (**10**-8 to **10**-16 and **11**-12 to **11**-16) showed enantiotropic liquid-crystalline properties and the detailed transition temperatures for these complexes are provided in Table 2 and the behaviour is summarised in Figure 8. Thus complexes **10**-n all show a Col_h phase as suggested by polarised optical microscopy (Figure 9a) and confirmed for **10**-16 by SAXS (see below). With the exception of **10**-16 which shows a melting point at 41 °C, it was not possible to observe a melting event by either microscopy or DSC (recorded down to –40 °C). Given that a melting point is observed for **10**-16, then the likelihood is that crystallisation is suppressed and a glass forms in preference as it is unlikely that such relatively small changes in alkyl chain length would depress the melting point so far. Clearing points, however, are effectively invariant for **10**-8 to **10**-12 and decrease at **10**-16 but not before showing an increase at **10**-14. Such behaviour is unexpected and to that end we have checked the data point several times to confirm that it is correct; it is difficult to account for this observation.

Comparing the two homologues of **11**-n, both again show a Col_h phase (Fig. 9b shows an optical texture), both show a small decrease in clearing point and, in common with series **10**-n, a melting point is observed only for the C_{16} homologue. However, when comparing **10**-n and **11**-n, it is clear that while the crystal phases seem to have similar stabilities, the columnar phase of **11**-n are significantly more stable and indeed have rather high clearing points, although on the timescales of the experiments conducted we saw no evidence of decomposition. This is also borne out by

some photophysical studies described below. While it is not possible to confirm with complete confidence why this is so, it is proposed that this is a consequence of better organisation of **11**-*n* in the mesophase, as there is reduced steric repulsion between complexes in the absence of the fused cyclopentene ring.

Table 2 Thermal data for terpyridine metal complexes

Compound	Metal (Ligand)	Transition	$T/°C$	$\Delta H/kJ\ mol^{-1}$
10-8	Zn(**8**)	Col$_h$ – Iso	190	§
10-10	Zn(**8**)	Col$_h$ – Iso	194	§
10-12	Zn(**8**)	Col$_h$ – Iso	191	§
10-14	Zn(**8**)	Col$_h$ – Iso	221	§
10-16	Zn(**8**)	Cr – Col$_h$	41	78.8
		Col$_h$ – Iso	160	§
11-12	Zn(**9**)	Cr – Col$_h$	13	9.3
		Col$_h$ – Iso	286	17.8
11-16	Zn(**9**)	Cr – Col$_h$	45	59.5
		Col$_h$ – Iso	254	8.5
12-16	Rh(**8**)	Cr – Col$_r$	55	95.0
		Col$_r$ – Iso	250	4.0
13-16	Ir(**8**)	Cr – Col$_r$	40	63.3
		Col$_r$ – Iso	250	§
14-16	Rh(**9**)	Cr – Col$_h$	40	51.0
		Col$_h$-Col$_r$	175	9.3
		Col$_r$ – Iso	258	11.0
15-16	Ir(**9**)	Cr – Col$_h$	37	24.2
		Col$_h$-Col$_r$	170	4.3
		Col$_r$ – Iso	223	§
16-16	Eu(**8**)	Cr – Col$_h$	14	43.9
		Col$_h$ – Iso	110	§
18-16	Eu(**9**)	Cr – Col$_h$	49	92.8
		Col$_h$ – Iso	172	§
19-12	Dy(**9**)	Col$_h$ – Iso	220	6.5
20-16	Co(**8**)	Cr – Col$_h$	46	79.8
		Col$_h$ – Iso	144	§
21-16	Co(**9**)	Cr – Col$_h$	50	97.5
		Col$_h$ – Iso	218	§

Cr = crystal; Col$_h$ = columnar hexagonal phase; Col$_r$ = columnar rectangular phase (although see text discussion); Iso = isotropic liquid.

§ Peaks either not seen or poorly resolved.
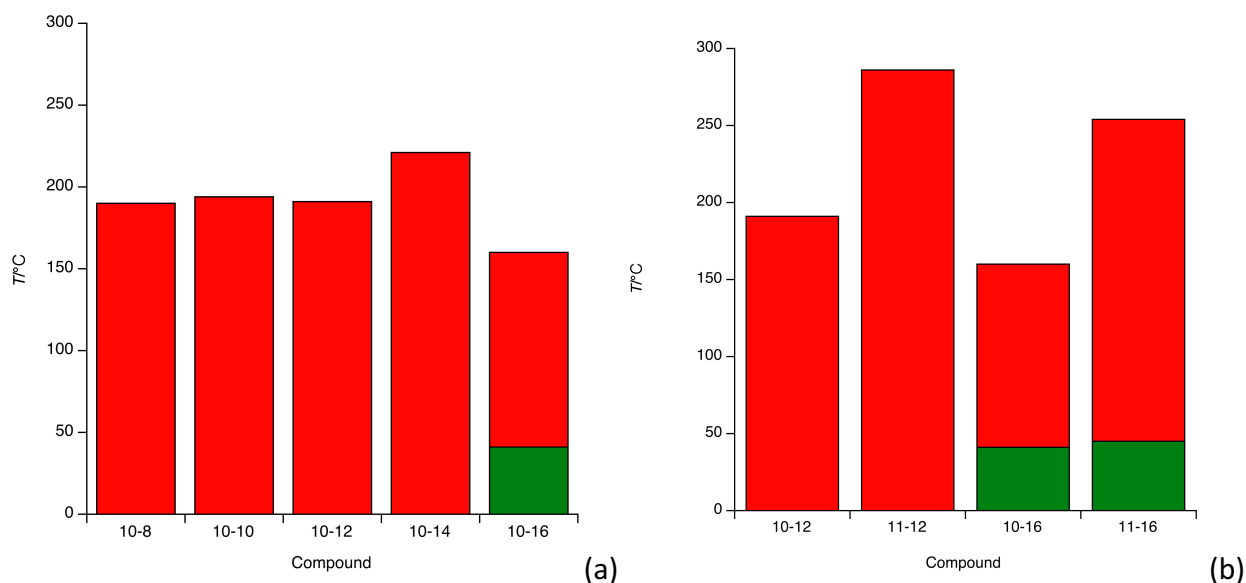
Figure 8   (a) Phase behaviour of complexes **10**-*n* and (b) comparison of the transition temperatures of two homologues of **10**-*n* and **11**-*n*. Red = Col$_h$ and green = Crys.
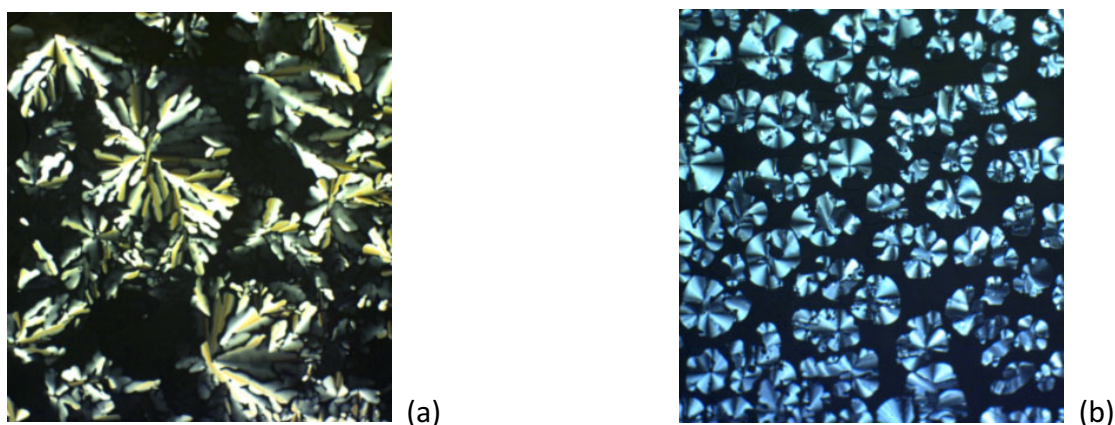
Figure 9   Polarizing microscopic textures obtained for: a) **10**-16 at 207 °C in cooling cycle and b) **11**-16 at 245 °C in cooling cycle.

The X-ray diffraction pattern obtained for **11**-12 showed a strong peak at a low angle corresponding to a *d*-spacing of 27.27 Å and a broad and a diffuse maximum in the wide angle corresponding to a *d*-spacing of 4.6 Å (Fig. 10a). Distinct peaks were also seen in the small-angle regime and were found to be in the ratio 1: √3: √4:√7: √9, which can be identified as arising from a two-dimensional hexagonal lattice of a columnar order and indexed as the (10), (11), (20), (21), (30), (40) and (32) reflections, respectively, with a lattice parameter *a* = 31.12 Å. A broad halo observed at higher angles could be resolved into two diffuse peaks corresponding to spacings of 4.6 and 3.6 Å. The former peak is due to the molten alkyl chains, while the second arises due to a

−17−

repeating of aromatic along the columnar axis. In conjunction with the image from polarised optical microscopy, the data for **10**-12 also revealed a Col$_h$ phase except that this one showed fewer reflections. Furthermore, the lattice parameter was 39.26 Å and there was no evidence of a reflection corresponding to ring stacking at 3.6 Å. Comparison of the two is consistent with a more compact arrangement of **11**-12, which is readily rationalised on account of the absence of the fused C$_5$ rings. The more compact arrangement would also be expected to be expressed as a more stable mesophase for **11**-12, which is also observed.

On the basis of the X-ray data, it is difficult, indeed perhaps unwise, to speculate too much on the organisation within the mesophases, although clearly, as half-disc materials, there are some assumptions that can be made in order that space is filled. From this viewpoint, while it is dangerous to make links between solid-state structures and mesophase organisation, it is possible that the back-to-back arrangement seen in the single-crystal structure of **10**-1 (Figure 6) provides some hints. This arrangement is similar to that proposed by Morale *et al.* in half-disc, hexacatenar 2,6-bis(phenylimino)pyridines.[13]

Rh^{III} and Ir^{III} Complexes

All complexes showed enantiotropic columnar mesophases with a wide mesomorphic range and the detailed transition temperatures for these complexes are provided in Table 2. The mesophases of these materials were very viscous and so it was not possible to obtain good textures for phase identification, which then relied on X-ray data. Thus, the pairs of Rh^{III} and Ir^{III} complexes, namely **12**-16 and **14**-16 (Rh with and without the fused C$_5$ ring, respectively), and **13**-16 and **15**-16 (Ir with and without the fused C$_5$ ring, respectively) show mesomorphism that is dependent on the ligand, but with rather little effect of the metal. Thus, **12**-16 and **13**-16 show very similar melting points and identical clearing points, and the X-ray data reveal the presence of a Col$_r$ phase with *c2mm* symmetry; the lattice parameters are very close in value (Rh: a = 72.6 Å, b = 35.1 Å; Ir: a = 72.24 Å, b = 35.52 Å). Similarly, the mesomorphism of **14**-16 and **15**-16 are very similar, with both showing a lower-temperature Col$_h$ phase and a higher-temperature Col$_r$ phase

with *p2mm* symmetry (Fig. 10b). The temperatures of the Cr-Col$_h$ and Col$_h$-Col$_r$ transitions are extremely similar (Table 2), while the two clearing points are very close as are the two sets of lattice parameters (*e.g.* for Col$_r$ – Rh: a = 59.26 Å, b = 39.59 Å; Ir: a = 58.88 Å, b = 39.17 Å). In these cases, the ligand has little effect on the clearing points, which may be due the great steric demands of the Cl ligands on the metal with two M–Cl vectors perpendicular to the ligand plane.
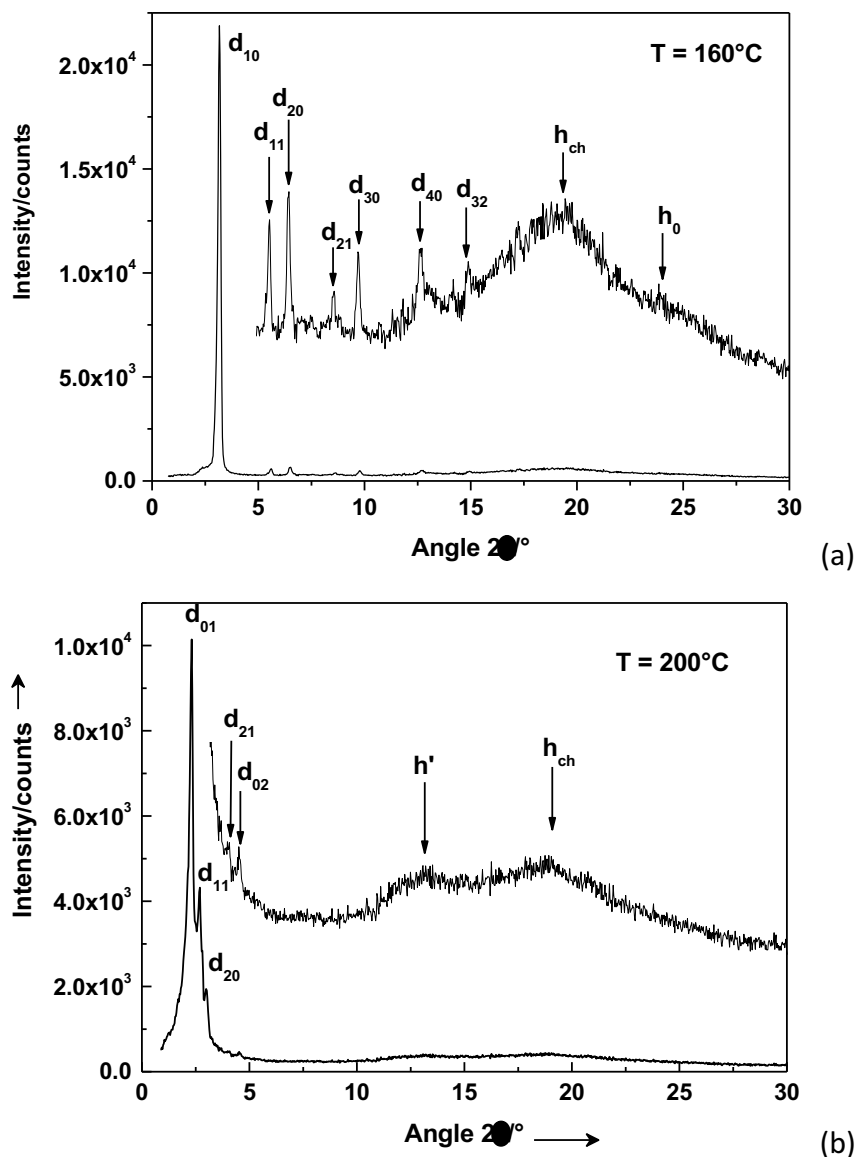
Figure 10. X-ray diffraction pattern of; a) **11**-12 at 160 °C and b) **14**-16 at 200 °C. Inset shows the corresponding XRD pattern obtained at higher 2θ region.

A feature of interest with **14**-16 and **15**-16 is the appearance of a rectangular phase above the hexagonal. In fact, while the symmetry of this mesophase is indeed rectangular, it does not belong

to the same symmetry group of commonly encountered Col$_r$ phases (*i.e. c2mm* or *p2gg*). In the present case the phase is of a lower symmetry, and can be visualised as a lamellar phase with antiperistaltic undulations.[16a] We may argue that on increasing the temperature, the volume of the chains increases substantially and, since they are connected to the aromatic core, the divergence from a flat-layer structure and the induction of undulations[16b] appears to be the best compromise found in order to remain self-organised before eventually melting to the isotropic liquid.

Table 3. X-ray diffraction data of complexes, presenting the measured and calculated spacing, Miller indices and lattice dimensions

Compound	$d_{meas.}$/Å	I	hk	d_{calc}	parameters
10-12	34.0	VS (sh)	10	34.0	T = 160 °C
	4.6	VS (br)	–	h_{ch}	
					Col$_h$
					a = 39.26 Å
					S = 1335 Å^2
11-12	27.27	VS (sh)	10	26.95	T = 160 °C
	15.67	S (sh)	11	15.56	
	13.44	S (sh)	20	13.47	Col$_h$
	10.20	M (sh)	21	10.18	a = 31.12 Å
	8.97	M (sh)	30	8.98	S = 838.7 Å^2
	6.85	M (sh)	40	6.73	
	5.98	M (sh)	32	6.18	
	4.6	VS (br)	–	h_{ch}	
	3.6	S (br)	–	h_0	
11-16	30.35	VS (sh)	10	30.45	T = 140 °C
	17.6	S (sh)	11	17.58	
	15.25	S (sh)	20	15.22	Col$_h$
	4.6	VS (br)	–	h_{ch}	a = 35.16 Å
					S = 1070.6 Å^2
14-16	39.3	VS (sh)	10	39.18	T = 160 °C
	22.7	M (br)	11	22.62	Col$_h$
	19.46	W (sh)	20	19.59	a = 45.24 Å
	7.0	S (br)	–	h'	S = 1772.5 Å^2
	4.6	VS (br)	–	h_{ch}	
	38.9	VS (sh)	01	39.05	T = 200°C
	32.92	S (sh)	11	32.9	Col$_r$-*p2mm*
	29.63	S (sh)	20	29.6	a =59.26 Å
	23.0	W (sh)	21	23.7	b = 39.59 Å
	19.75	M (sh)	02	19.79	S = 2346 Å^2
	6.8	S (br)	–	h'	
	4.6	VS (br)	–	h_{ch}	
15-16	38.54	VS (sh)	10	38.58	T = 140 °C
	22.3	M (br)	11	22.27	Col$_h$
	7.0	S (br)	–	h'	a = 44.55 Å
	4.6	VS (br)	–	h_{ch}	S = 1718.6 Å^2

	d_{obs}	I	hk	d_{calc}	Parameters
	38.95	VS (sh)	01	39.17	T = 180 °C
	32.6	S (sh)	11	32.6	Col$_r$-$p2mm$
	29.4	S (h)	20	29.4	a =58.8 Å
	6.9	S (br)	–	h'	b = 39.17 Å
	4.6	VS (br)	–	h_{ch}	S = 2303.3 Å^2
12-16	36.3	S (sh)	20	36.3	T = 180 °C
	31.57	VS (sh)	11	31.6	Col$_r$-$c2mm$
	18.26	S (sh)	40	18.15	a = 72.6 Å
	15.26	M (sh)	22	15.8	b = 35.1 Å
	13.72	S (sh)	51	13.42	S = 2548 Å^2
	12.73	S (sh)	42	12.61	
	10.55	W (sh)	33	10.53	
	6.8	S (br)	–	h'	
	4.6	VS (br)	–	h_{ch}	
13-16	36.12	S (sh)	20	36.1	T = 140 °C
	31.88	VS (sh)	11	31.9	Col$_r$-$c2mm$
	19.24	S (sh)	31	19.93	a = 72.24 Å
	18.1	S (sh)	40	18.06	b = 35.52 Å
	15.9	S (sh)	22	15.94	S = 2566 Å^2
	13.3	M (sh)	51	13.38	
	12.55	S (sh)	42	12.66	
	12.06	S (sh)	60	12.04	
	11.19	S (sh)	33	11.25	
	9.6	W (sh)	71	9.9	
	6.7	S (br)	–	h'	
	4.7	VS (br)	–	h_{ch}	
16-16	42.88	VS (sh)	10	43.05	T = 120 °C
	24.95	S (sh)	11	24.85	Col$_h$
	7.0	S (br)	–	h'	a = 49.71 Å
	4.6	VS (br)	–	h_{ch}	S = 2140 Å^2
18-16	39.8	VS (sh)	10	39.8	T = 100 °C
	6.8	S (br)	–	h'	Col$_h$
	4.6	VS (br)	–	h_{ch}	a = 45.95 Å
					S = 1830 Å^2
19-12	34.1	VS (sh)	10	34.0	T = 140 °C
	19.6	S (sh)	11	19.64	Col$_h$
	7.0	S (br)	–	h'	a = 39.37 Å
	4.6	VS (br)	–	h_{ch}	S = 1342.7 Å^2

Eu^{III} and Dy^{III} complexes

In common with the Rh^{III} and Ir^{III} complexes, these lanthanide complexes are also very viscous and it was not possible to use optical microscopy to gain a definitive characterisation of the mesophases formed and so X-ray diffraction was again used.

It is found that **16**-16 (Eu) shows a Col$_h$ phase as evidenced by the observation of both a (10) and (11) reflection, with evidence for a Eu···Eu correlation at 7 Å and a stacking period of 3.6 Å. The observation of the stacking period is interesting in comparison to some of the observations above as the ligand here contains the fused C$_5$ rings and the metal bears the three bulky κ^2-nitrato ligands, which would imply some sort of back-to-back arrangement of the complexes in the mesophase. The data for **18**-16 (Eu) and **19**-12 (Dy) show a single reflection in the low-angle region; optical textures did not help resolve the question of phase symmetry. However, as a rectangular phase can be ruled out and as both the M···M separations and the lattice parameters calculated assuming a Col$_h$ phase (and taking into account the shorter chain length in **19**-12) tally well with those of **16**-16, then these phases are also assigned as Col$_h$.

Co^{III} complexes

In common with several of the materials described above, the cobalt complexes did not give useful optical textures by microscopy and so while it was possible to discern the melting and clearing points in this way, phase characterisation relied on SAXS data. The two complexes melted at very similar temperatures just above ambient (Table 2), but showed rather different thermal phase stabilities so that the complex (**21**-16) with the functionalised ligand **9**-16 cleared almost 70 °C higher than **20**-16. SAXS data showed that both complexes exhibited a Col$_h$ phase with almost identical lattice parameters ($a \approx 39$ Å) so that the structural data do not provide a clue to the significant difference in mesophase stability between the two complexes.

That a complex of this type leads to liquid crystal formation is of some interest, not least because of the known spin-crossover behaviour associated with Co^{III} and Co^{III} complexes and N_6 ligand donor sets, including terpyridine.[17] An example of a related liquid-crystalline Co^{II} complex with an N_6 donor set derived from pyridine-2,6-diimine ligands has been reported recently and exhibited spin-crossover properties;[18] other examples of possible or actual liquid-crystalline complexes of cobalt with spin-crossover properties have been reported.[19] The data for the X-ray structure of **20**-

1 were recorded at 110 K and then again at room temperature[†] so that bond lengths could be compared. Despite the much larger esds in the room-temperature structure, it was evident from the Co–N bond lengths that there was no spin-crossover behaviour in the range 298-110 K. Nonetheless, with tuning *via* the ligand, such complexes in due course represent an avenue for development in combining liquid crystal and magnetic properties.

Photophysical Properties in Solution

Photophysical properties were determined for complexes of Zn[II] (**10**-16 and **11**-16) and Ir[III] (**13**-16 and **15**-16) as now described. However, no significant emission was observed for the Eu complexes (**16**-16 and **18**-16), which is attributed to quenching of the Eu excited state by coordinated water.[20]

Zinc(II) Complexes

Two representative zinc(II)-terpyridine complexes with hexadecyl chains were chosen for preliminary photophysical studies, one with (**10**-16) and one without (**11**-16) a fused cyclopentene ring. Absorption and emission studies were carried out in solvents of varying polarity and data are collected in Table 4. The normalised absorption spectra of **10**-16 in different solvents are shown in Figure 11a and λ_{max} appears to be almost independent of solvent polarity which is an indication that the dipole moments of the ground and excited states are very similar and the transitions are predominantly ligand centred (see calculations below). For **11**-16, the absorption maxima show a small hypsochromic shift with increasing solvent polarity (see Figure 11b); a broadening of the absorption curve, particularly on the low-energy shoulder, was observed in non-polar solvents such as cyclohexane.

[†] Structure 1423114 in the Cambridge database.

The behaviour of the emission spectra is different in that there is a pronounced hypsochromic shift in the emission maximum of **10**-16 as solvent polarity is reduced, whereas for **11**-16 there is a much smaller *bathochromic* shift (see Figs. 11c and 11d). Lifetime measurements confirm the singlet nature of the excited state.
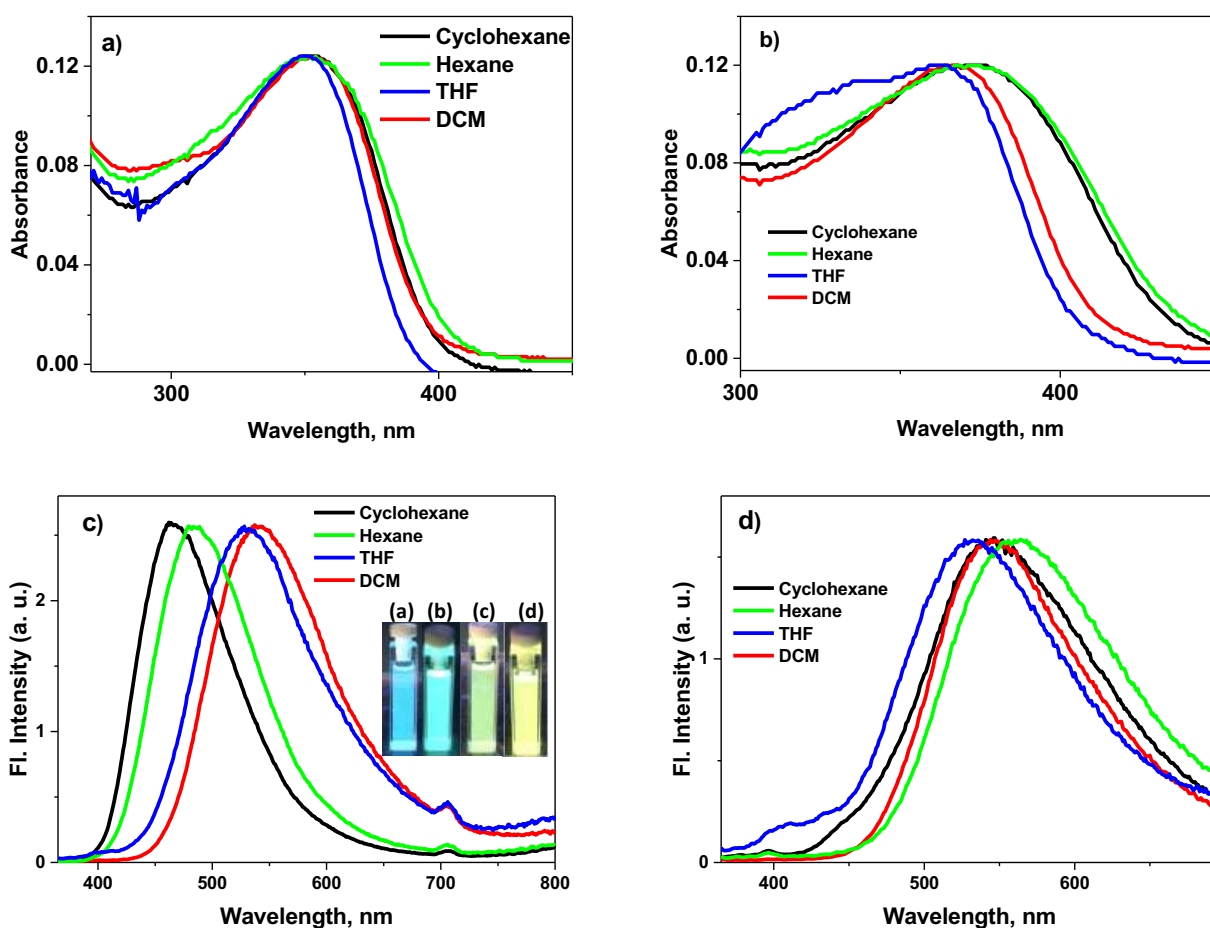
Figure 11. Normalised absorption spectra of a) **10**-16 and b) **11**-16 in different solvents; Normalised emission spectra of c) **10**-16 and d) **11**-16; λ_{ex} = 354 nm. Figure c inset shows solutions of **10**-16 under illumination at 376 nm in: a) cyclohexane; b) hexane; c) THF and d) CH_2Cl_2.

It is also of note that the emission quantum yields vary between **10**-16 and **11**-16 and as a function of solvent. Thus for **10**-16, quantum yields of between 0.3-0.4 are found in hexane and cyclohexane, decreasing to 0.08 in THF and CH_2Cl_2. The decrease observed in the more polar solvents is consistent with emission from a charge-transfer state (see below) because of high rate of non-radiative processes as a result of high degree of stabilisation of charge transfer state. That

the quantum yields for **11**-16 are not sensitive to solvent reflects the slightly different nature of the excited state as discussed below.

Table 4. The photophysical data for zinc(II) complexes in various solvents

Solvents	$\lambda_{max(abs)}$/nm		$\lambda_{max(em)}$/nm		$\varepsilon \times 10^{-3}$/M^{-1} cm^{-1}		ϕ*		τ (ns)	
	10-16	**11**-16	**10**-16	**11**-16	**10**-16	**11**-16	**10**-16	**11**-16	**10**-16	**11**-16
Hexane	353	373	484	557	29.28	26.34	0.302	0.049	6.09	5.53
Cyclohexane	353	375	464	546	30.72	26.46	0.394	0.083	7.00	6.00
THF	351	363	529	532	34.15	33.40	0.081	0.051	2.35	1.30
DCM	353	368	541	546	34.50	30.25	0.081	0.062	3.65	2.07

*Reference used for QY measurement is *tris*(2,2'-bipyridyl)ruthenium(II) (ϕ = 0.042)

Calculation of the Photophysical Properties of the Zinc(II) Complexes

In order to obtain a better understanding of the solvatochromic properties of complexes **10**-*n* and **11**-*n*, density functional theory (DFT) calculations were performed on simplified models in which the terminal chains were substituted by methyl groups so as to reduce computational effort. Geometry optimisations of ground states (S$_0$) were carried out using Gaussian09[21] at the M06-2X/aug-cc-pVDZ level of theory with a dense 'SuperFine' integration grid, under the 'VeryTight' convergence criteria, and the optimised geometries were identified as local minima through calculations of analytical harmonic vibrational frequencies. For each of the two complexes two local minima corresponding to distinct conformers were found on potential energy surface, in agreement with the XRD experimental data for complex **10**-1. The difference between the conformers is in the twisting of the two terminal trialkoxyphenyl groups: For each complex one conformer exhibits C_s symmetry, with the trialkoxyphenyl groups twisted in different directions ('disrotation') relative to the terminal pyridines to which they are bound, while the second conformer has no symmetry and the trialkoxy groups are twisted in the same direction ('conrotation') (see Figure 12). All four conformers were observed to have very flat potential energy surfaces around the optimised geometries, with lowest vibrational frequencies of just 9.7

cm^{-1} and 9.1 cm^{-1} for the C_s symmetry conformers and of just 6.5 cm^{-1} and 8.5 cm^{-1} for the conformers with no symmetry of complexes **10**-1 and **11**-1, respectively. As a result of this feature, reliable convergence in the S_0 geometry optimisations could only be achieved through the use of basis sets including diffuse functions.
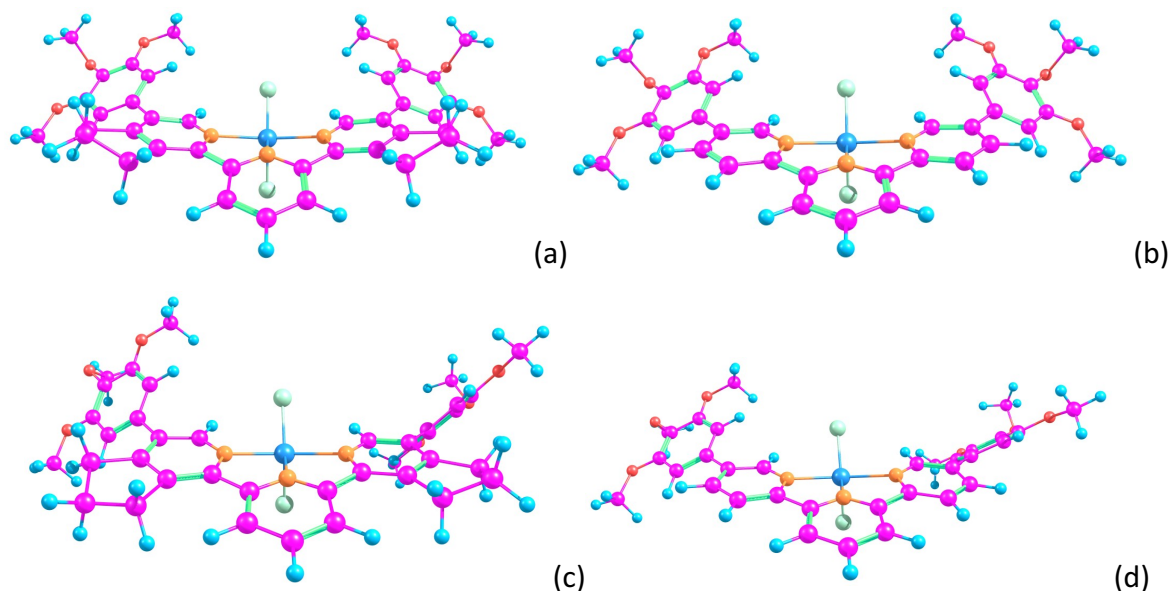

Figure 12. Optimised ground state geometries of conformers with C_s symmetry (top structures), and with no symmetry (bottom structures) of complexes **10**-1 (on the left) and **11**-1 (on the right) calculated at the M06-2X/aug-cc-pVDZ level of theory.

A detailed comparison of the differences between the two conformers for each complex is given in the Supplementary Information, but one point of note is that while from the single crystal structure determination of **10**-1, and indeed the other complexes reported here, there is asymmetry in the Zn–N bond lengths (with that from the central pyridine shortest in all but one structure), the calculations show all three Zn–N bond lengths as essentially identical. Finally here, according to the calculations, in the case of complex **11**-1, the conformation with no symmetry appears to be slightly more stable than its C_s symmetry partner, by 2.0 kJ mol^{-1} (<kT @ 298 K), whereas for complex **10**-1 the conformer with C_s symmetry is more stable than the conformer with no symmetry by 13.6 kJ mol^{-1}.

The calculated wavelengths corresponding to vertical excitations from the ground state S_0 to the first singlet excited state S_1 in the gas phase are 308.25 nm and 307.74 nm (**10**-1), and 316.62 nm and 316.87 nm (**11**-1), for conformers of C_s symmetry and conformers with no symmetry, respectively. These S_1 calculations were carried out at the time-dependent (TD) M06-2X/cc-pVDZ level with the 'SuperFine' integration grid, at the M06-2X/aug-cc-pVDZ S_0 geometries and the results show that the two types of conformer are not distinguishable by absorption. The values obtained for the $S_0 \rightarrow S_1$ transition wavelengths are shorter than the longest wavelength experimental absorption maxima in chloroform by 42 nm (**10**-1) and 58 nm (**11**-1), respectively. The computational results also indicate that the dipole moments in all four conformers are directed from the negatively charged chloride anions and electron-donor trialkoxyphenyl groups towards the terpyridine moiety, with magnitudes, for the conformers exhibiting C_s symmetry, of 13.66 D (S_0) and 9.83 D (S_1) for **10**-1, and 12.41 D (S_0) and 8.12 D (S_1) for **11**-1; the values for the conformers without symmetry were obtained as 10.96 D (S_0) and 5.60 D (S_1) for **10**-1, and 9.54 D(S_0) and 4.36 D (S_1) for **11**-1. Thus, in both complexes, the conformers with C_s symmetry exhibit larger S_0 and S_1 dipole moments in comparison to the conformers with no symmetry.

Next, the geometries of the first singlet excited states (S_1) of all the four conformers were optimised at the TDM06-2X/cc-pVDZ level using again the 'SuperFine' integration grid, but under the 'Tight' criteria, as it was not possible to achieve reliable convergence to geometries satisfying the stricter 'VeryTight' criteria. The optimised S_1 geometries show that, as a result of the structural relaxation following a vertical excitation, the conformers with C_s symmetry become flatter, as the dihedral angles between the trialkoxyphenyl groups and the pyridine rings attached to these groups decrease from 37.78° to 28.74°, and from 34.88° to 23.00° for **10**-1 and **11**-1, respectively. The S_1 structural relaxation in the conformers with no symmetry follows a different pattern. Here again the dihedral angles between the trialkoxyphenyl groups and neighbouring pyridine groups are observed to decrease, from 45.86° to 32.99° and from 50.60° to 44.33° for **10**-1; from 35.3° to 30.92° and from 36.92° to 36.38° for **11**-1. However, the S1 geometries do not become flatter as in the case of the C_s symmetry conformers, but assume more helical shapes due

to a twisting at the coordination center which is not observed for conformers of C_s symmetry (see Figure 13).
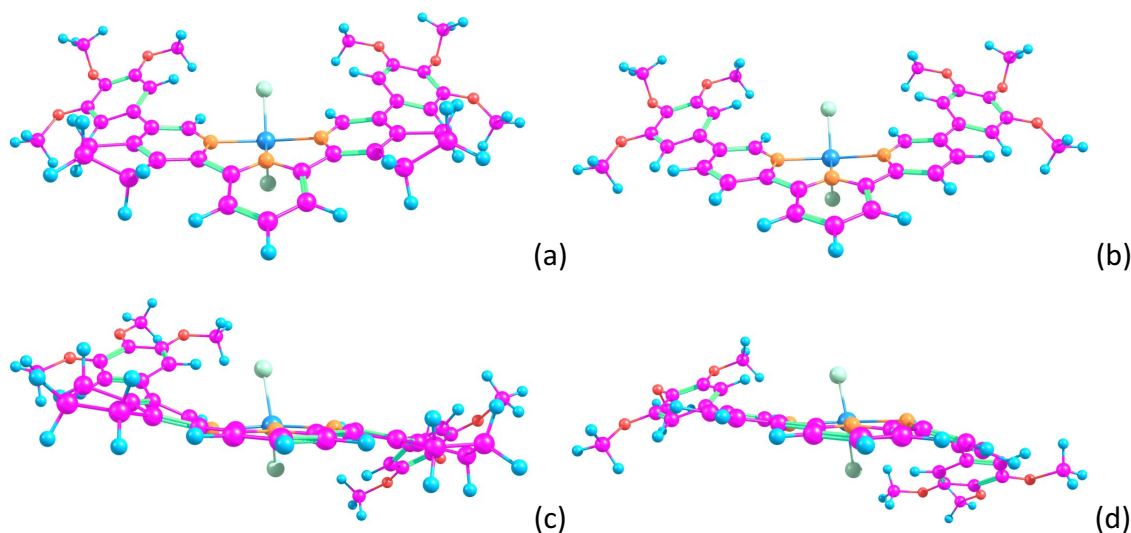

Figure 13. Optimised S_1 geometries of conformers with Cs symmetry (top structures), and with no symmetry (bottom structures) of complexes **10**-1 (pm the left) and **11**-1 (on the right), calculated at the TDM06-2X/cc-pVDZ level of theory.

The dipole moments of the C_s symmetry conformers at the S_1 optimised geometries were obtained as 9.37 D (**10**-1) and 8.36 D (**11**-1) exhibiting, as a result of the S_1 structural relaxation, slight reductions of 0.46 D and 0.24 D, respectively. For the conformers without symmetry, after the S_1 geometry optimisations, the S_1 dipole moments jump to 11.71 D (**10**-1) and to 12.42 D (**11**-1), showing differences of 6.11 D (**10**-1) and 8.06 D (**11**-1) from the S_1 dipole moments calculated at the S_0 geometries.

Additional calculations on the S_1 states were carried out at the S_0 and S_1 geometries obtained with Gaussian09 by means of ORCA 3.0.3,[22] at the TDM06-2X/cc-pVDZ and TDB3LYP/cc-pVDZ levels of theory, using the 'GRID7' integration grid. The results obtained at the TDM06-2X/cc-pVDZ level of theory level show excellent agreement with those coming from Gaussian09.

The TDB3LYP/cc-pVDZ calculations at the S_0 geometries, however, yield gas phase $S_0 \rightarrow S_1$ transition wavelengths of 412.6 nm and 420.6 nm (**10**-1), and of 424.8 nm and 422.2 nm (**11**-1),

for conformers with C_s symmetry and with no symmetry, respectively. These wavelengths are longer than the longest wavelength absorption determined in chloroform solution. The TDB3LYP/cc-pVDZ calculations also produce ground state dipole moments of 12.80 D and 9.94 D for complex **10**-1, and of 11.52 D and 8.82 D for complex **11**-1, for conformers with C_s symmetry and with no symmetry, respectively. The S_1 dipole moments were obtained as 6.11 D and 4.59 D (**10**-1), and as 4.53 D and 4.25 D (**11**-1), for conformers with C_s symmetry and without symmetry, respectively.

The isosurface plots of the electron density differences between the S_0 and S_1 states obtained at the TDM06-2X/cc-pVDZ level of theory at the S_0 geometries show that in all conformers the S_1 state exhibits intra-ligand charge transfer (ILCT) character, because electron density is transferred from the two trialkoxyphenyl groups to the terpyridine moiety within the organic ligand (see Figure 14).

If use is made of the optimised S_1 geometries, the electron density difference distribution remains much the same as that obtained at the S_0 geometries for the conformers with C_s symmetry. However, for the conformers with no symmetry, the excited state electron density migrates to one side of the molecule (see Figure 13 for the geometry), which is obviously the reason for the much larger S_1 dipole moments at the S_1 optimised geometries (see Figure 15).
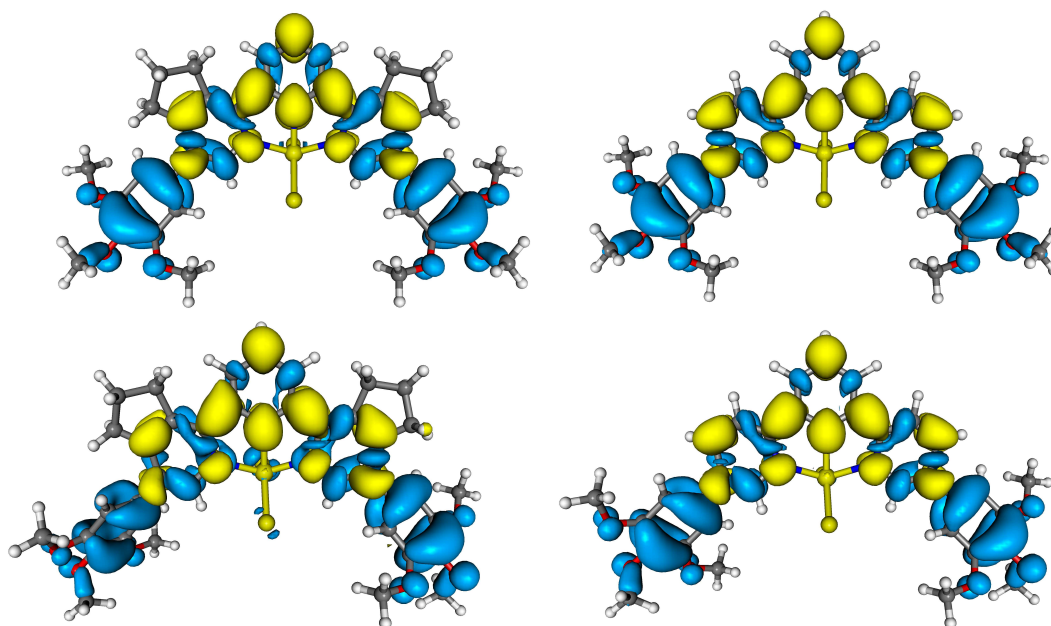
Figure 14. Isosurface plots of the electron density differences between the S_0 and S_1 states of conformers with C_s symmetry (top plots), and with no symmetry (bottom plots) for complexes **10**-1 (on the left) and **11**-1 (on the right), calculated at the TDM06-2X/cc-pVDZ level of theory at the S_0 geometries. Yellow/blue correspond to areas of increased/reduced electron density in S_1 in comparison to S_0 (isovalues of ±0.0005).

Figure 15. Isosurface plots of the electron density differences between the S_0 and S_1 states of conformers with C_s symmetry (top plots), and with no symmetry (bottom plots) of complexes **10**-1 (on the left) and **11**-1 (on the right), calculated at the TDM06-2X/cc-pVDZ level of theory at the S_1 optimised geometries. Yellow/blue correspond to areas of increased/reduced electron density in S_1 in comparison to S_0 (isovalues of ±0.0005).

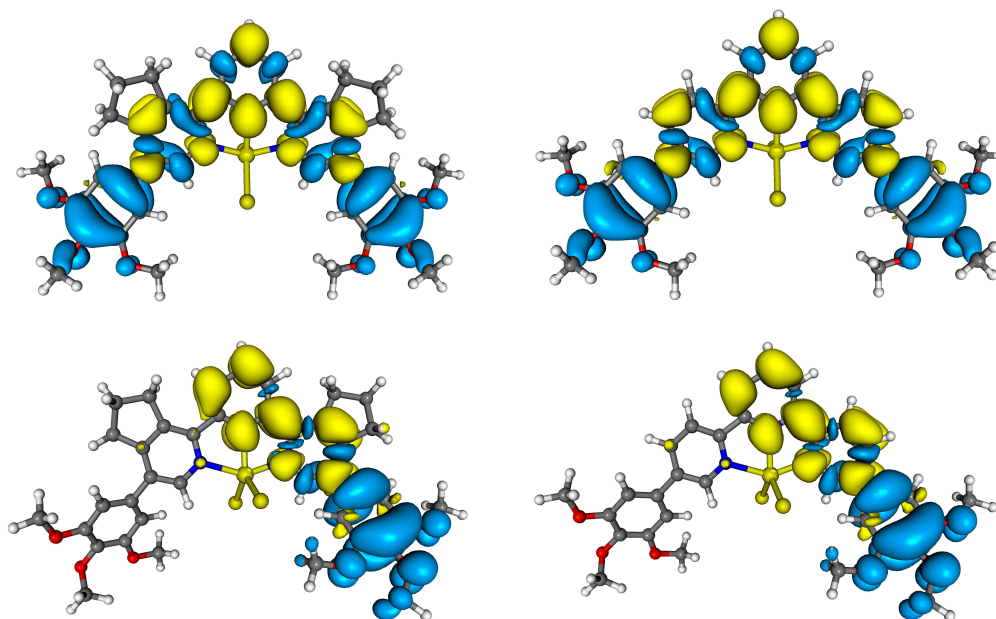However, the analogous isosurface plots of the electron density differences between the S_0 and S_1 states obtained at the TDB3LYP/cc-pVDZ level of theory at the S_0 geometries show a different

picture. Thus, in all conformers the S_1 state exhibits ligand to ligand charge transfer (LLCT) character, because electron density is transferred from chlorine anions in the $ZnCl_2$ unit to the terpyridine moiety, which also reduces the dipole moments at the S_1 geometries (see Figure S9). It is obvious that the isosurface plots of the electron density differences between the S_0 and S_1 states are affected significantly by the choice of the exchange-correlation functional; on the whole, use of M06-2X with complexes **10**-1 and **11**-1 ensures better agreement with experiment than that afforded by B3LYP.

The experimentally observed solvatochromism can then be accounted for using data obtained at TDM06-2X/cc-pVDZ level of theory for the more stable conformers of **10**-1 (C_s symmetry) and **11**-1 (no symmetry) at the respective S_0 geometries. As mentioned already, the corresponding S_1 dipole moments are 9.83 D (**10**-1) and 4.36 D (**11**-1). However, the computational results suggest that the $ZnCl_2$ unit does not participate in the formation of the S_1 state and, as a consequence, the solvation shell of this unit cannot stabilise this excited state. Calculations on $ZnCl_2$ units at the same level of theory level at geometries 'cut out' from those for the respective complexes produce dipole moments of 3.79 D (**10**-1, C_s symmetry) and 3.97 D (**11**-1, no symmetry). The differences between the dipole moments of the whole complex in the S_1 state and those of the $ZnCl_2$ units provide estimates of the dipole moments of the organic ligands in the S_1 states, namely 6.04 D (**10**-1, C_s symmetry) and 0.39 D (**11**-1, no symmetry) (ignoring minor differences in direction). The very small dipole moment of 0.39 D on the moiety which is most active in the formation of the excited state can explain the slight hypsochromic shift upon emission (destabilisation of the excited state), observed for **11**-1 when increasing the polarity of the solvent, while the corresponding value of 6.04 Debye for **10**-1 is quite high and consistent with the observed bathochromic shift upon emission (stabilisation of the excited state) observed when increasing the polarity of the solvent. Moreover, for complex **11**-1, a $ZnCl_2$ unit solvation shell of polar molecules can destabilise the S_1 state even more by being too rigid to allow reorganisation.

It should be emphasised that charge transfer within the organic ligand (ILCT) for the S_1 state is observed only when the M06-2X functional is used, which is accompanied by an increased energy

of the $S_0 \rightarrow S_1$ transition in comparison to the experimental measurement. Calculations on the S_1 state using the B3LYP functional show charge transfer from the auxiliary chlorine ligands to the terpyridine moiety of the organic ligand (LLCT), accompanied by lower than the experimentally measured energies for the $S_0 \rightarrow S_1$ transitions. Thus, in reality, the S_1 states can have characteristics intermediate between the predictions of the M06-2X and B3LYP models and may exhibit mixed ILCT/LLCT nature. If this is so, because of the geometry differences, the contributions of ILCT and LLCT to **10**-1 and **11**-1 will not be comparable, leading to different quenching of the active dipole moment, which can be reduced to a value close to zero in **11**-1, and increased in **10**-1; these effects could provide an alternative explanation of the differences in the solvatochromic properties of the two complexes.

Iridium(III) Complexes

The absorption and emission properties of two Ir complexes, **13**-16 and **15**-16, were determined at room temperature in two solvents of different polarity; poor solubility in other solvents limited the scope of this investigation. The complexes absorbed (Figure 16) at *ca* 364 nm for **13**-16 and 370 nm for **15**-16, with a slightly shorter-wavelength absorption for **13**-16 owing to the reduced conjugation in the terpy ligand. An extinction coefficient value of 10^4-10^5 M^{-1} cm^{-1} was observed, which is consistent with a transition that is predominantly ligand centred (^{1}LC).[23] The room-temperature luminescence for degassed solutions of the Ir[III] complexes in the two solvents was studied (λ_{ex} = 415 nm) and it was found that **13**-16 emits strongly with emission maxima of 621 nm and 605 nm in hexane and CH_2Cl_2, respectively, a decrease of 16 nm with increasing solvent polarity indicating that the solvent plays a considerable role in luminescence behaviour of the complex. A similar shift in emission wavelength was also observed for **15**-16 in the same solvents, although this complex is much less emissive. The detailed absorption and emission maxima, Stokes shift, molar extinction coefficient and quantum yield in different solvents are collected in Table 5.

Complexes **13**-16 and **15**-16 give long excited-state lifetimes (τ) in degassed solutions and lifetimes of 0.7 μs and 0.8 μs in DCM, and 1.5 μs and 1.2 μs in hexane, respectively, were obtained. In second- and third-row transition metal complexes, emission from the triplet state, normally formally forbidden, is promoted through high spin–orbit coupling of the metal ions, the extent of which depends on the participation of metal orbitals in the excited state.[24] The broad emission bands exhibited by the Ir[III] complexes without vibronic structure indicates that they originate from the [3]MLCT transition state.[24] This contrasts with the behaviour of the unsubstituted complex [Ir(terpy)Cl$_3$][25] where emission is from a [3]LC excited state. However, Collin *et al.*[23b] reported that for complexes of the type [Ir(terpy')$_2$]$^{3+}$ (terpy' = a 4-phenyl-substituted terpy), the extended conjugation of the ligand caused the emission to change to [3]MLCT. For purely organic molecules, k_r for the lowest lying triplet state is typically only around 1–10[3] s^{-1}, whereas for a given metal ion, [3]MLCT excited states will typically have higher k_r values than [3]LC states. The k_r values calculated for **13**-16 and **15**-16 are provided in Table 3 and reveal the involvement of a [3]MLCT excited state in the luminescent behaviour of iridium complexes **13**-16 and **15**-16.

One thing of note is the quantum yields for emission for **13**-16, which are extremely high for Ir complexes of this type and also significantly higher than those found for **15**-16. This mirrors the situation with the Zn[II] complexes where the presence of the fused cyclopentene ring in the ligand again leads to higher emission quantum yields. The origin of this effect (seen also in related complexes of platinum(II)[7e]) is not presently clear, but may be due to an increased rigidity of the ligand, removing some non-radiative relaxation pathways.

Table 5. The photophysical data of iridium(III) complexes in various solvents

Solvents	$\lambda_{max(abs)}$/nm		$\lambda_{max(em)}$/nm		$\varepsilon \times 10^{-3}$/M^{-1} cm^{-1}		k_r (10[5] s^{-1})		ϕ*		τ/μs	
	13-16	**15**-16	**13**-16	**15**-16	**13**-16	**15**-16	**13**-16	**15**-16	**13**-16	**15**-16	**13**-16	**15**-16
CH$_2$Cl$_2$	364	369	605	605	26.66	26.34	4.2	0.63	0.30	0.05	0.7	0.8
Hexane	369	378	621	622†	30.41	26.46	2.6	0.66	0.40	0.08	1.5	1.2

*Reference used for QY measurement is *tris*(2,2'-bipyridyl)ruthenium(II) (ϕ = 0.042)
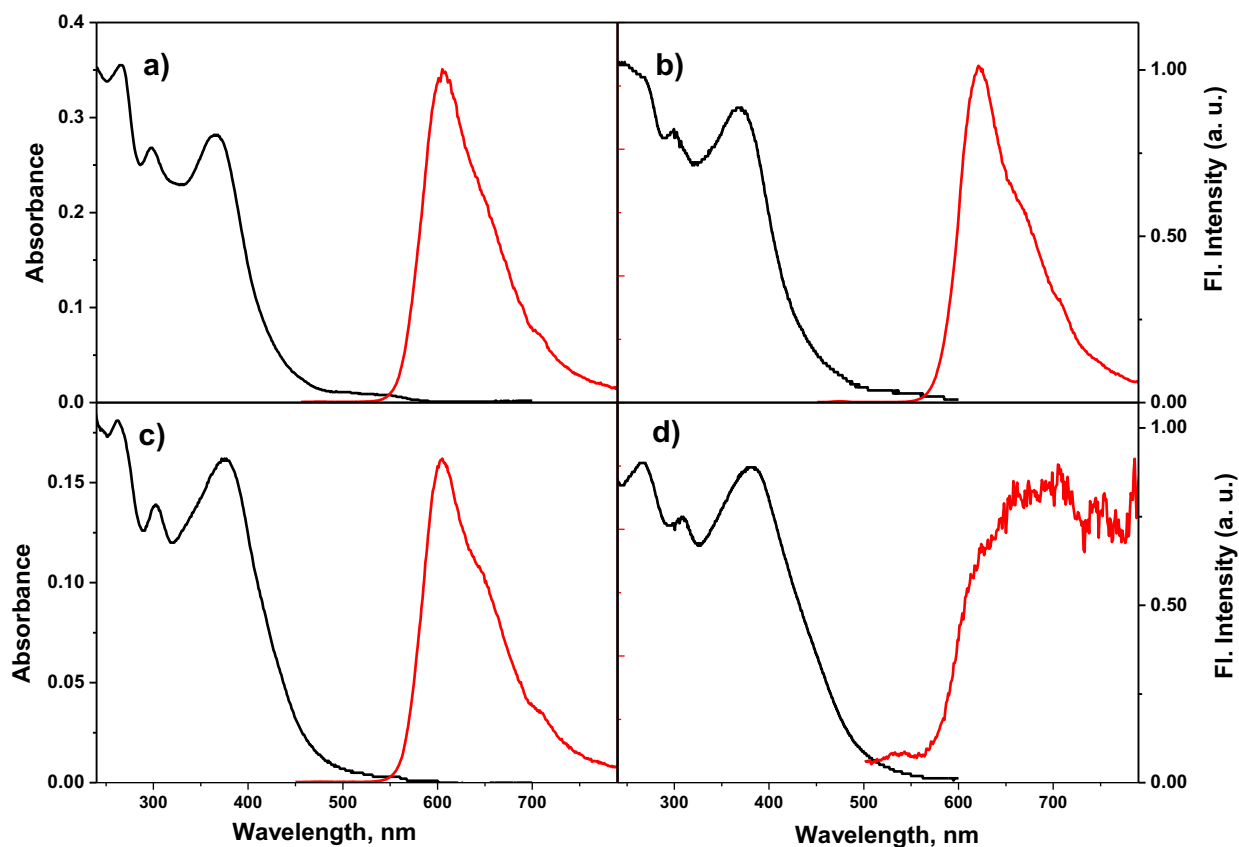
† Very weak.

Figure 16. The normalised absorption (black) and emission (red) spectra of Ir^{III} complexes. a) **13**-16 in DCM; b) **13**-16 in hexane; c) **15**-16 in DCM and d) **15**-16 in hexane. λ_{ex} = 415 nm.

Photophysical properties in the solid state

Zinc(II) Complexes

The solid-state luminescence of the Zn^{II} complexes was analysed from spin-coated films obtained for each derivative from chloroform solution. Prepared this way, complex **10**-16 emits at room temperature with a maximum at 509 nm, whereas **11**-16 emits strongly at 545 nm, both upon excitation at 386 nm. The effect of temperature on the fluorescence behaviour of these complexes was investigated by keeping the films at different temperatures for 30 minutes and suddenly cooling by withdrawing them to room temperature on a metal plate to effect rapid heat

dissipation (and hence cooling). That this method is appropriate and effective is borne out by the results below. Thus, for complex **10**-16, there were no noticeable changes in the emission maxima for these cooled films and the corresponding normalised spectra are provided in Figure 17a. The related excitation spectra (Figure 17c) also show no variation with preparation temperature, all of which suggests that there is no ground state aggregate between complexes. For complex **11**-16 however, a hypsochromic shift was observed for emission maxima of cooled films annealed at higher temperatures, with greater shifts from films cooled from higher temperatures (Figure 17b). The excitation spectra (Figure 17d) also show a temperature dependence. This suggests that **11**-16 aggregates at room temperature leading to a red shift in emission and that when the temperature increases, the aggregates break apart into monomeric form leading to a blue shift in the emission maximum.

To provide support for this hypothesis, luminescent studies on **11**-16 were carried out in the solid state (as a powder) and dispersed in PMMA films. Thus, the powdered form of compound **11**-16 was sealed between two microscope cover slips and its luminescence was measured at different temperatures. In the powdered state, **11**-16 emits strongly with a maximum at 565 nm, but a 42 nm hypsochromic shift was observed when the temperature was increased reaching 523 nm at 254 °C at which temperature the complex enters the isotropic phase (Figure S1). The corresponding excitation spectra also showed a hypsochromic shift in the emission maxima, indicating clearly that there is ground-state aggregation between molecules. When dispersed in PMMA, **11**-16, from 100 wt% to 50 wt% of **11**-16, there was no significant shift in the emission maximum at room temperature, whereas hypsochromic shifts of 19 nm and 32 nm were observed for films doped with 25% and 10% complex, respectively (Figure S2). The change in emission at different temperatures for **11**-16 doped into PMMA was then analysed by keeping the films at a particular temperature for 30 minutes and then cooling rapidly to room temperature. A hypsochromic shift was observed once the heated films were cooled, clearly confirming that compound **11**-16 aggregates in both powder form and at higher concentrations in PMMA doped films, changing to its monomeric form upon dilution with PMMA as well as with increasing temperature. The excitation spectra overlap well in all the above cases. Figure 18a and 18b shows

the fluorescent images obtained for these complexes (**10**-16 and **11**-16) under 365 nm illumination.
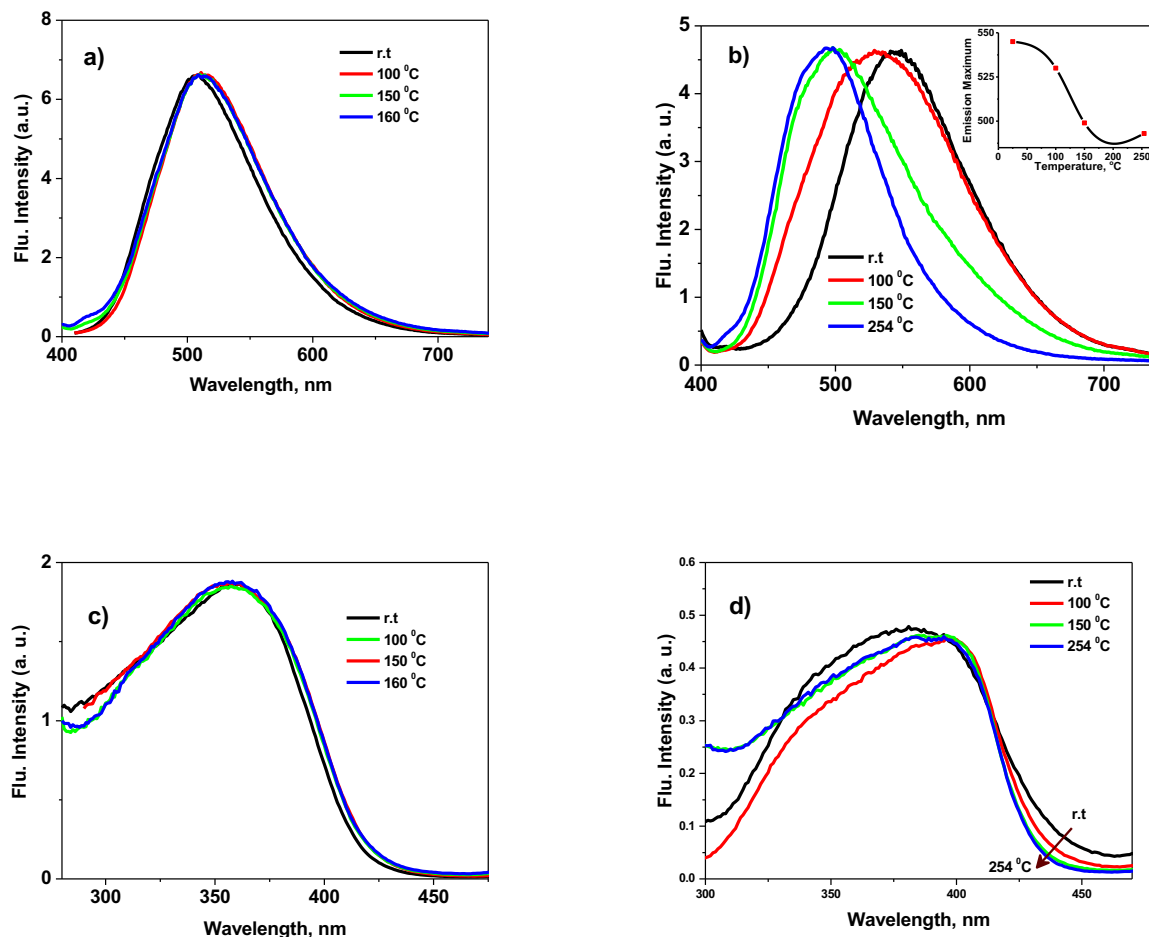
Figure 17. Normalised emission spectra of spin coated films prepared from chloroform solvent; a) **10**-16 and b) **11**-16; λ_{ex} = 386 nm. Normalised excitation spectra of same films for; c) **10**-16 and d) **11**-16; λ_{em} = 500 nm. Figure **11**-16 inset shows the change in emission maximum with increase of temperature for spin-coated film.

Figure 18. The fluorescent images obtained for a) **10**-16; b) **11**-16 and c) **13**-16 in their spin-coated films under 365 nm illumination.

Iridium(III) Complexes

The photophysical properties of the Ir[III] complexes were also studied in spin-coated films prepared from chloroform so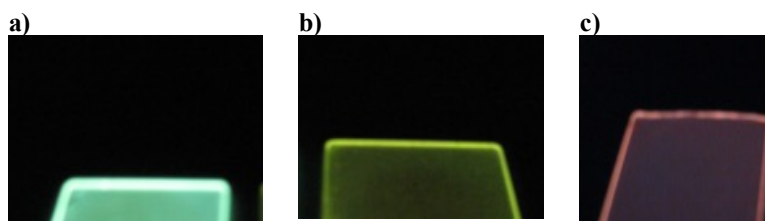lution. Thin films of complex **13**-16 emit in the red region with an emission maximum at 619 nm, whereas complex **15**-16 hardly emits at all. The effect of temperature on the luminescence properties of films of **13**-16 at different temperatures was also studied by following the same experimental procedures outlined above for Zn[II] complexes. Up to 100 °C, there was no change in the luminescence maximum, whereas a 36 nm bathochromic shift was observed at 176 °C for the same film upon excitation with 375 nm light (Figure 19a); on isotropisation the luminescence was quenched completely (blue trace in Figure 19a). The normalised excitation spectra at different temperatures (Figure 19b) showed no significant shift in the emission maxima indicating that there was no ground-state aggregate formation. Therefore it seems that the 36 nm shift is attributable to a reorganisation consequent on entering the liquid crystal phase (see below) and generating an excimer-like emission. The insensitive nature of the excitation spectrum at different temperatures also suggests that the emission could arise from the excimer-like species and indeed there are reports in the literature in which an excimer-like emission is observed for metal complexes in their liquid-crystalline phase.[7e] To confirm the origin of this behaviour, temperature-dependent luminescent studies of **13**-16 were undertaken by sealing the sample between two microscope cover slips. Done in the powdered form, the compound emits with maxima at 595 and 630 nm suggesting that there are different modes of packing in the solid state (Figure 19c). However, at 160 °C the peak at 595 nm decreased in intensity with a concomitant increase in the emission intensity at 630 nm showing that the organisation associated with the longer-wavelength emission is that found also in the liquid crystal state and indeed by 175 °C, all emission was found at 630 nm. The fact that all emission was not at 630 nm at 160 °C despite the compound being in the liquid-crystalline state is likely a reflection of paramorphosis in which aspects of the solid-state organisation persist (seen often in the polarised optical microscopy). Further increases in temperature (to 260 °C), led to the formation of an isotropic liquid and complete quenching of the luminescence.

A comparative study of temperature-dependent emission behaviour of spin-coated films of 100% **13**-16 with 99% PMMA-doped films were also studied (Figure 19d). The results showed that the bathochromic shift at 175 °C was exclusively for the pure film, and the emission did not vary with temperature for the doped PMMA films. The corresponding excitation spectra in all these cases confirmed that there is no ground state aggregation between the molecules (see Figure S4) supporting the proposal of excimer formation in the liquid crystal phase. The reason for **13**-6 to show red shifted emission (λ_{max}= 650 nm) compared to emission maximum observed at 630 nm in the powder state could be due to the difference in molecular arrangement of the compound in thin film. Figure 18c shows the fluorescent image obtained for complex **13b** under 365 nm illumination.
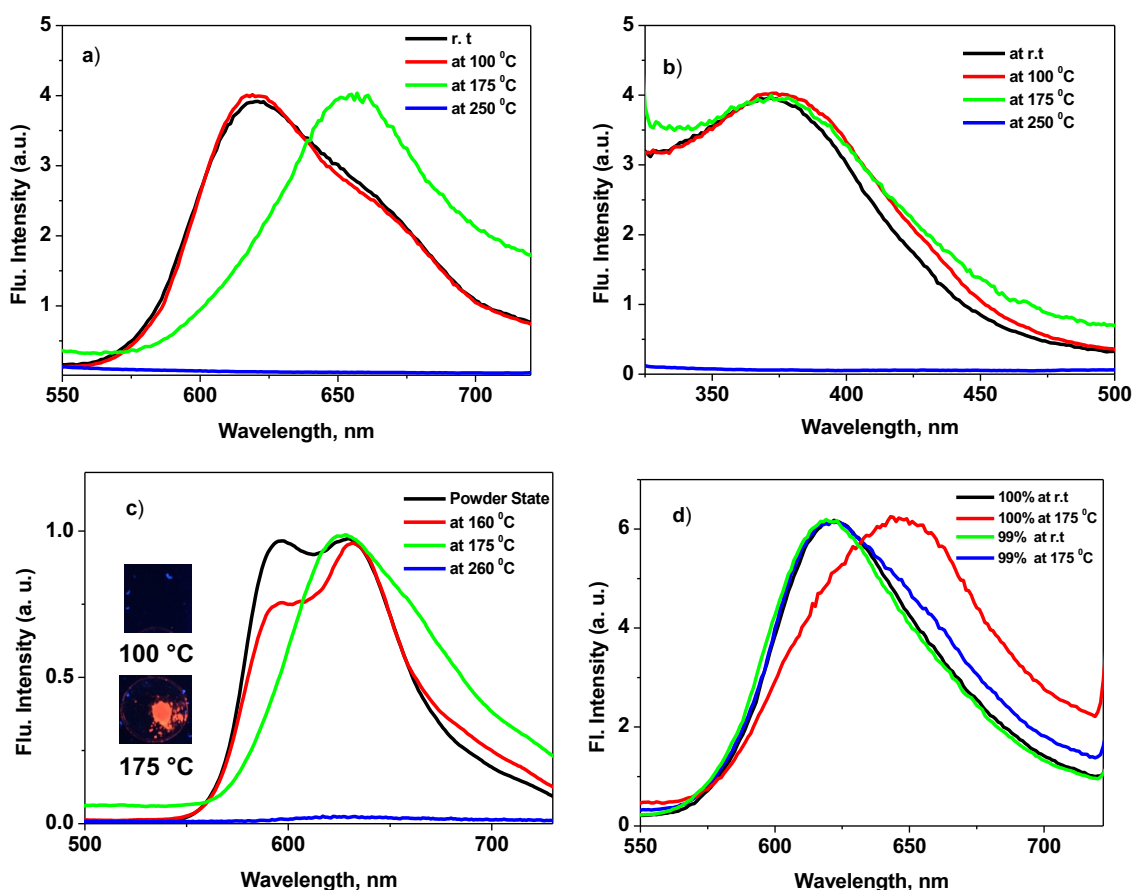
Figure 19. a) Normalised emission spectra of spin coated film of **13**-16 at different temperatures – λ_{ex} = 375 nm; b) normalised excitation spectra of the same film at different temperatures – λ_{em} = 620 nm; c) normalised emission spectra of **13**-16 in powder form and at different temperatures – λ_{ex} = 375 nm; d) comparison of emission spectra of thin films of **13**-16 in pure film and in PMMA doped film – λ_{ex} = 375 nm.

Conclusion

Through the synthetic flexibility offered by Boger chemistry, two series of hexaalkoxy-substituted 2,2′:6′,2′′terpyridines were prepared: a) one with a fused cyclopentene ring attached to each lateral pyridyl and b) one without such rings. They were then complexed to a range of metals to give 5- (Zn^{II}), 6- (Rh^{III}, Ir^{III}, Co^{III}) and 9-(Eu^{III}, Dy^{III}) coordinate complexes, all with liquid crystal properties. Coordinate geometries were verified by single crystal X-ray diffraction (except for Rh^{III}). Despite the range of coordination numbers, geometries and metal:ligand stoichiometries, the ligands were able to induce columnar liquid crystal mesophases, which extended in many cases from ambient to temperatures above 200 °C and which were characterised by in-mesophase small-angle X-ray scattering. Of particular interest in this regard were the 2:1 complexes of Co^{III} as this represents a very uncommon coordination mode in realizing metallomesogens. For some metal systems, differences in thermal stability of the mesophases was observed as a function of the ligand type, attributed to the ability of the complexes to stack, whereas in others there was little or no difference suggesting that other steric factors were at work associated with coordination around the metal ion.

While complexes of Eu^{III} were perhaps surprisingly not luminescent, something attributed to excited state deactivation by coordinated water, the complexes of Zn^{II} and Ir^{III} were luminescent in solution, in the solid state and in the mesophase. Emission from the zinc complexes was from a singlet state, while for iridium it was from the triplet manifold. Zinc complexes of the terpy ligands with fused cyclopentene rings (**10**-*n*) showed significant solvatochromism, which was not seen in the related complexes (**11**-*n*) without this fused ring. Investigations using DFT and TD-DFT calculations suggested that the contrasting behaviour arose owing to significant differences in the dipolar nature of the two excited states.

In the solid and liquid crystal state, there were evident changes in the emission wavelength as a function of temperature, which is attributable to different levels of organisation in the materials,

so that the method of preparation and fabrication, plus the added variable of temperature, gives appreciable control of the emission characteristics.

Thus, the ligands used in this study show a remarkable ability to promote liquid crystal behaviour when complexed to a wide range of metals where the liquid crystallinity extends over a very wide temperature range. Moreover, many of the complexes are luminescent – some with singlet and some with triplet emission – and there is evidence that the degree of organisation over which there is control *via* the phase in which the material is found (and hence the temperature) can be controlled, thus controlling the emission characteristics.

Acknowledgements

References

1. a) R. H. Crabtree, *The Organometallic Chemistry of the Transition Metals* 6th edn., Wiley, New York, 2014; b) J. P. Collman, L. S. Hegedus, J. R. Norton, R. G. Finke, *Principles and Applications of Organotransition Metal Chemistry,* University Science Books, Mill Valley CA, 1987.

2. a) A. Harriman, R. Ziessel, *Coord. Chem. Rev.* **1998**, *171*, 331-339. b) V. Balzani, *Electron Transfer in Chemistry*. Vol. 1-5, Wiley-VCH, Weinheim, 2001; c) A. Kaifer, M. G. Kaifer, *Supramolecular Electrochemistry* (Wiley-VCH), 2007. d) N. Robertson, C. A. McGowan, *Chem. Soc. Rev*. **2003**, *32*, 96- 103; e) F. Barigelletti, L. Flamigni, *Chem. Soc. Rev*. **2000**, *29*, 1-12.

3. a) B. O'Regan, M. Grätzel, *Nature* **1991**, *353*, 737-740; b) C. A. Bignozzi, R. Argazzi, C. J. Kleverlaan, *Chem. Soc. Rev.* **2000**, *29*, 87-96; c) M. Grätzel, *Nature* **2001**, *414*, 338-344; d)

M. K. Nazeeruddin, M. Grätzel, J. A. McCleverty, T. J. Meyer (Eds.), in *Comprehensive Coordination Chemistry II.*, vol. 9. pp. 719-758, Elsevier-Pergamon, Oxford, 2004.

4. a) H. Yersin, *Highly Efficient OLEDs with Phosphorescent Materials*. Wiley-VCH. 2007; b) E. Holder, B. M. W. Langeveld, U. S. Schubert, *Adv. Mater*. **2005**, *17*, 1109- 1121; c) M. A. Baldo, D. F. O'. Brien, Y. You, A. Shoustikov, S. Sibley, S. R. Thompson, S. R. Forrest, *Nature* **1998**, *395*, 151- 154; d) C. S. K. Mak, A. Hayer, S. I. Pascu, S. E. Watkins, A. B. Holmes, A. Koehler, R. H. Friend, *Chem. Commun.* **2005**, 4708- 4710; e) F. G. Gao, A. J. Bard, J*. Am. Chem. Soc.* **2000**, *122*, 7426- 7427; f) J.-K. Lee, D. S. Yoo, E. S. Handy, M. F. Rubner, *Appl. Phys. Lett.* **1996**, *69*, 1686- 1688; g) S. Graber, K. Doyle, M. Neuburger, C. E. Housecroft, E. C. Constable, R. D. Costa, E. Ortí, D. Repetto, H. J. Bolink, *J. Am. Chem. Soc.* **2008**, *130*, 14944- 14945; h) C.-H. Yang, Y.-M. Cheng, Y. Chi, C.-J. Hsu, F.-C. Fang, K.-T. Wong, P.-T. Chou, C.-H. Chang, M.-H. Tsai, C.-C. Wu, *Angew. Chem. Int. Ed.* **2007**, *46*, 2418- 2421.

5. a) S. J. Lippard, J. M. Berg, *Principles of Bioinorganic Chemistry*. University Science Books, Mill Valley, 1994; b) H. Dürr, S. Bossmann, *Acc. Chem. Res.* **2001**, *34*, 905- 917; c) M. Sykora, K. A. Maxwell, J. M. DeSimone, T. J. Meyer, *Proc. Nat. Acad. Sci. USA* **2000**, *97*, 7687- 7691; d) W. Kühlbrandt, D. N. Wang, Y. Fujiyoshi, *Nature* **1994**, *367*, 614-621; e) H. Inoue, S. Funyu, Y. Shimada, S. Takagi, *Pure. Appl. Chem.* **2005**, *77*, 1019- 1033; f) V. Balzani, L. De Cola, Eds. *Supramolecular Chemistry*; NATO ASI Series; Kluwer Academic Publishers: Dordrecht, 1992; g) J. Barber, B. Andersson, *Nature* **1994**, *370*, 31-34; h) V. K. Yachandra, K. Sauer, M. P. Klein, *Chem. Rev.* **1996**, *96*, 2927- 2950; i) M. R. Wasielewski, *Chem. Rev*. **1992**, *92*, 435- 461.

6. a) A. M. Prokhorov, A. Santoro, J. A. G. Williams, D. W. Bruce, *Angew*. *Chem*. *Int*. *Ed*. **2012**, *51*, 95- 98; b) A. Santoro, A. M. Prokhorov, V. N. Kozhevnikov, A. C. Whitwood, B. Donnio, J. A. Williams, D. W. Bruce, *J. Am*. *Chem*. *Soc.* **2011**, *133*, 5248- 5251; c) P.-H. Lanoë, C. M. Tong, R. W. Harrington, M. R. Probert, W. Clegg, J. A. G. Williams, V. N. Kozhevnikov, *Chem*. *Commun*. **2014**, *50*, 6831- 6834; d) Y. Zheng, A. S. Batsanov, M. A. Fox, H. A. Al-Attar, K. Abdullah, V. Jankus, M. R. Bryce, A. P. Monkman, *Angew*. *Chem*. *Int*. *Ed*. **2014**, *53*, 11616- 11619; e) N. M. Shavaleev, G. Xie, S. Varghese, D. B. Cordes, A. M. Z. Slawin, C. Momblona, E. Ortí, H. J. Bolink, I. D. W. Samuel, E. –Z. Colman, *Inorg*. *Chem*. **2015**, *54*, 5907–5914; f) R.

D. Costa, E. Ortí, H. J. Bolink, F. Monti, G. Accorsi, N. Armaroli, *Angew*. *Chem*. *Int*. *Ed*. **2012**, *51*, 8178- 8211; g) D. N. Kozhevnikov, V. N. Kozhevnikov, M. Z. Shafikov, A. M. Prokhorov, D. W. Bruce, J. A. G. Williams, *Inorg*. *Chem*. **2011**, *50*, 3804–3815.

7. a) V. W-W. Yam, V. K-M. Au, S. Y-L. Leung, *Chem*. *Rev*. **2015**, *115*, 7589; b) Y. Wang, J. Shi, J. Chen, W. Zhu, E. Baranoff, *J*. *Mater*. *Chem*. *C* **2015**, *3*, 7993- 8005; c) M. Krikorian, S. Liu, T. M. Swager, *J*. *Am*. *Chem*. *Soc*. **2014**, *136*, 2952–2955; d) D. N. Kozhevnikov, V. N. Kozhevnikov, M. M. Ustinova, A. Santoro, D. W. Bruce, B. Koenig, R. Czerwieniec, T. Fischer, M. Zabel, H. Yersin, *Inorg*. *Chem*. **2009**, *48*, 4179-4189; e) V. N. Kozhevnikov, B. Donnio, D. W. Bruce, *Angew*. *Chem*. *Int*. *Ed*. **2008**, *47*, 6286- 6289; f) A. Santoro, A. C. Whitwood, J. A. G. Williams, V. N. Kozhevnikov, D. W. Bruce, *Chem*. *Mater*. **2009**, *21*, 3871- 3882; g) M. Spencer, A. Santoro, G. R. Freeman, Á. Díez, P. R. Murray, J. Torroba, A. C. Whitwood, L. J. Yellowlees, J. A. G. Williams, D. W. Bruce, *Dalton Trans*. **2012**, *41*, 14244- 14256; h) Á. Díez, S. J. Cowling, D. W. Bruce, *Chem*. *Commun*. **2012**, *48*, 10298- 10300.

8. a) E. Cariati, E. Lucenti, C. Botta, U. Giovanella, D. Marinotto, S. Righetto, *Coord*. *Chem*. *Rev*. **2016**, *306*, 566-614; b) X.-L. Chen, C.-S. Lin, X.-Y. Wu, R. Yu, T. Teng, Q.-K. Zhang, Q. Zhang, W.-B. Yang, C.-Z. Lu, *J*. *Mater*. *Chem*. *C*, **2015**, *3*, 1187–1195; c) C. Bizzarri, C. Strabler, J. Prock, B. Trettenbrein, M. Ruggenthaler, C.-H. Yang, F. Polo, A. Iordache, P. Brüggeller, L. De Cola, *Inorg*. *Chem*. **2014**, *53*, 10944–10951.

9. a) K. Binnemans, *J*. *Mater*. *Chem*. **2009**, *19*, 448–453; b) R. Bayón, S. Coco, P. Espinet, *Chem*. *Eur*. *J*. **2005**, *11*, 1079- 1085; b) E. Cavero, S. Uriel, P. Romero, J. L. Serrano, R. Gimnez, *J*. *Am*. *Chem*. *Soc*. **2007**, *129*, 11608- 11618; c) Y. Yang, K. Driesen, P. Nockemann, K. V. Hecke, L. V. Meervelt, K. Binnemans, *Chem*. *Mater*. **2006**, *18*, 3698- 3704.

10. A. Escande, L. Guénée, H. Nozary, G Bernardinelli, F. Gumy, A. Aebischer, J.-C. G. Bünzli, B. Donnio, D. Guillon, C. Piguet, *Chem*. *Eur*. *J*. **2007**, *13*, 8696- 8713; E. Terazzi, S. Torelli, G. Bernardinelli, J. -P. Rivera, J. -M. Bénech, C. Bourgogne, B. Donnio, D. Guillon, D. Imbert, J. -C. G. Bünzli, A. Pinto, D. Jeannerat, C. Piguet *J*. *Am*. *Chem*. *Soc*. **2005** *127* 888-903; H. Nozary, S. Torelli, L. Guénée, E. Terazzi, G. Bernardinelli, B. Donnio, D. Guillon, C. Piguet *Inorg*. *Chem*. **2006** *45* 2989-3003; E. Terazzi, L. Guénée, P.-Y. Morgantini, G. Bernadinelli, B. Donnio, D. Guillon, C. Piguet *Chem*. *Eur*. *J*. **2007** *13* 1674-1691; E. Terazzi, S. Torelli, G.

Bernardinelli, J.-P. Rivera, J.-M. Bénech, C. Bourgogne, B. Donnio, D. Guillon, D. Imbert, J.-C. G. Bünzli, A. Pinto, D. Jeannerat, and C. Piguet, *J. Am. Chem. Soc.*, **2005**, *127*, 888-903; H. Nozary, C. Piguet, P. Tissot, G. Bernardinelli, J.-C. Bünzli, R. Deschenaux and D. Guillon, *J. Am. Chem. Soc.*, **1998**, *120*, 12274-12288.

11. R. A. A.; Foster, M. C. Willis, *Chem. Soc. Rev.*, **2013**, *42*, 63-76.

12. a) V. N.; Kozhevnikov, D. N.; Kozhevnikov, O. V.; Shabunina, V. L. Rusinov, O. N.,Chupakhin, *Tetrahedron Lett*. **2005**, *46*, 1791- 1793; b) V. N.; Kozhevnikov, D. N. Kozhevnikov, T. V.; Nikitina, V. L. Rusinov, O. N.; Chupakhin, M.; Zabel, B. König, *J. Org. Chem.* **2003**, *68*, 2882- 2888; c) V. N.; Kozhevnikov, S. C.; Cowling, P. B.; Karadakov, D. W., Bruce, *J. Mater. Chem.* **2008**, *18*, 1703-1710; e) V. N.; Kozhevnikov, A. C. Whitwood, D. W. Bruce, *Chem. Commun*. **2007**, 3826- 3828; f) A. Wild, A. Winter, F. Schlütter, U. S. Schubert, *Chem*. *Soc*. *Rev*. **2011**, *40*, 1459–1511; g) U. S. Schubert, H. Hofmeier, G. R. Newkome, *Modern Terpyridine Chemistry*, Wiley-VCH: Weinheim, Baden-Wurtemberg, Germany, 2006.

13. F. Morale, R. W. Date, D. Guillon, D. W. Bruce, R. L. Finn, C. Wilson, A. J. Blake, M. Schröder, B. Donnio, *Chem*. *Eur*. *J.* **2003**, *9*, 2484- 2501.

14. A. L. Spek, *Acta Crystallogr.*, *Sect*. *D* **2009**, *65*, 148- 155.

15. a) K. Binnemans, in *Molecular Materials*, ed. Bruce, D. W.; O'Hare, D.; Walton, R. I., Wiley, Chichester, 2010, pp 61–141; b) J. L. Serrano, *Metallomesogens*: *Synthesis, Properties, and Applications*; VCH, Weinheim, 1996; p 498.

16. a) T. Cardinaels, J. Ramaekers, P. Nockemann, K. Driesen, K. Van Hecke, L. Van Meervelt, G. Wang, S. De Feyter, E. Fernandez Iglesias, D. Guillon, B. Donnio, K. Binnemans and D. W. Bruce, *Soft Matter*, **2008**, *4*, 2172–2185; b) A. I. Smirnova, B. Heinrich, B. Donnio and D. W. Bruce, *RSC Adv.*, **2015**, *5*, 75149–75159.

17. a) M. A. Halcrow, Ed.; *Spin-Crossover Materials*: *Properties and Applications*, Wiley, Chichester, 2013; b) Y. H. Lee, J. M. Harrowfield, J. W. Shin, M. S. Won, E. Rukmini, S. Hayami, K. S. Min, Y. Kim, *Int. J. Mol. Sci.* **2013**, *14*, 20729-20743; c) M. L. Scudder, H. A. Goodwin, I. G. Dance, *New J. Chem.*, **1999**, *23*, 695-705; d) J. McMurtrie, I. Dance, *CrystEngComm*, **2005**, *7*, 216–229; e) Y. Galyametdinov, V. Ksenofontov, A. Prosvirin, I. Ovchinnikov, G. Ivanova, P. Gütlich, W. Haase, *Angew*. *Chem*. *Int*. *Ed*. **2001**, *40*, 4269-4271.

18. N. Abdullah, N. L. M. Noor, A. R. Nordin, M. A. Halcrow, D. R. MacFarlane, M. A. Lazar, J. M. Pringle, D. W. Bruce, B. Donnio, B. Heinrich, *J. Mater*. *Chem*. *C* **2015**, *3*, 2491-2499.

19. a) P. Gütlich, H. A. Goodwin, *Topics Curr. Chem.* **2004**, *233*, 1; b) H. A. Goodwin, *Topics Curr. Chem.* **2004**, *234*, 23; c) R. P. Taylor, D. H. Templeton, A. Zalkin, W. D. HorrocksJr., *Inorg*. *Chem*., **1968**, *7*, 2629-2636

20. S. Lis, *J. Alloys Compd*. **2002**, *341*, 45-50

21. Gaussian 09, Revision D.01, M. J. Frisch, G. W. Trucks, H. B. Schlegel, G. E. Scuseria, M. A. Robb, J. R. Cheeseman, G. Scalmani, V. Barone, B. Mennucci, G. A. Petersson, H. Nakatsuji, M. Caricato, X. Li, H. P. Hratchian, A. F. Izmaylov, J. Bloino, G. Zheng, J. L. Sonnenberg, M. Hada, M. Ehara, K. Toyota, R. Fukuda, J. Hasegawa, M. Ishida, T. Nakajima, Y. Honda, O. Kitao, H. Nakai, T. Vreven, J. A. Montgomery, Jr, J. E. Peralta, F. Ogliaro, M. Bearpark, J. J. Heyd, E. Brothers, K. N. Kudin, V. N. Staroverov, R. Kobayashi, J. Normand, K. Raghavachari, A. Rendell, J. C. Burant, S. S. Iyengar, J. Tomasi, M. Cossi, N. Rega, J. M. Millam, M. Klene, J. E. Knox, J. B. Cross, V. Bakken, C. Adamo, J. Jaramillo, R. Gomperts, R. E. Stratmann, O. Yazyev, A. J. Austin, R. Cammi, C. Pomelli, J. W. Ochterski, R. L. Martin, K. Morokuma, V. G. Zakrzewski, G. A. Voth, P. Salvador, J. J. Dannenberg, S. Dapprich, A. D. Daniels, Ö. Farkas, J. B. Foresman, J. V. Ortiz, J. Cioslowski, D. J. Fox, Gaussian, Inc., Wallingford CT, 2009.

22. F. Neese, (2012) The ORCA program system, *Wiley Interdiscip*. *Rev*.: *Comput*. *Mol*. *Sci*., 2, 73-78.

23. a) J. A. G. Williams, A. J. Wilkinson, V. L. Whittle, *Dalton Trans.* **2008**, 2081-2099; b) J. –P. Collin, I. M. Dixon, J.-P. Sauvage, J. A. G. Williams, F. Barigelletti, L. Flamigni, *J. Am*. *Chem*. *Soc*. **1999**, *121*, 5009-5016.

24. K. S. Bejoymohandas, A. Kumar, S. Varughese, E. Varathan, V. Subramanian, M. L. P. Reddy, *J. Mater. Chem.* **2015**, *3*, 7405- 7420.

25. N. Yoshikawa, T. Matsumura-Inoue, *Anal*. *Sci*., **2003**, *19*, 761-765.